Hill's equation with quasi–periodic forcing: resonance tongues, instability pockets and global phenomena

Henk Broer * and Carles Simó †

In memoriam Ricardo Mañé

Abstract

A simple example is considered of Hill's equation $\ddot{x} + (a^2 + b\,p(t))x = 0$, where the forcing term p, instead of periodic, is quasi–periodic with two frequencies. A geometric exploration is carried out of certain resonance tongues, containing instability pockets. This phenomenon in the perturbative case of small $|b|$, can be explained by averaging. Next a numerical exploration is given for the global case of arbitrary b, where some interesting phenomena occur. Regarding these, a detailed numerical investigation and tentative explanations are presented.

Keywords: Schrödinger equation with quasi-periodic potential, (non-) reducibility to Floquet form, quasiperiodic resonance tongues and unstability pockets, positive Lyapunov exponent, collapse of resonance tongues and breakdown of tori.

Contents

*Dept. of Mathematics and Computer Science, University of Groningen, PO Box 800, 9700 AV Groningen, The Netherlands

†Dept. de Matemàtica Aplicada i Anàlisi, Universitat de Barcelona, Gran Via 585, 08007 Barcelona, Spain

1 Introduction

1.1 The setting

This paper studies Hill's equation with quasi–periodic forcing, given by

$$\ddot{x} + \Big(a^2 + b\,p(t)\Big)\; x = 0, \tag{1}$$

where a and b are parameters. The parametric forcing $p = p(t)$ is a quasi–periodic function $p(t) = P(t\omega_1, t\omega_2)$, for rationally independent frequencies ω_1, ω_2 and a double periodic and real analytic function $P : \mathbb{T}^2 \to \mathbb{R}$. To be precise, we mostly deal with the particular choice

$$p(t) = \cos(\omega_1 t) + \cos(\omega_2 t), \text{ or } P(\theta_1, \theta_2) = \cos(\theta_1) + \cos(\theta_2). \tag{2}$$

We take $\omega_1 = 1$ and $\omega_2 = \gamma$, where $\gamma = \frac{1}{2}(1 + \sqrt{5})$ is the golden number. Also certain perturbations of (2) will be considered. The parameter a is going to assume finite values, while for b we distinguish two cases. In the first, perturbative, case $|b|$ is taken small and we shall approach certain resonance phenomena by averaging techniques. In the second, global, case we present some explorative numerical results together with heuristic explanations.

Equation (1) can also be written as $-\partial^2 u/\partial x^2 - bV(x)u = a^2 u$, just replacing x by u and t by x. This is the classical Schrödinger equation (see, e.g. [10]) where V, the potential, replaces the previous function $p(t)$ and is quasiperiodic, and a^2 is the energy.

The second order equation (1) rewrites as a system

$$\begin{aligned}\dot{\theta} &= \omega, \\ \dot{x} &= y, \\ \dot{y} &= -(a^2 + b\,P(\theta))\,x,\end{aligned} \tag{3}$$

where $(\theta, (x, y)) \in \mathbb{T}^2 \times \mathbb{R}^2$ and where $\omega = (\omega_1, \omega_2)$. Observe that the 2–torus $\mathbb{T}^2 \times \{(0,0)\}$, given by $x = y = 0$, is invariant with quasi–periodic flow of frequency vector ω. The first aim of this study is to investigate the normal linear behaviour of this invariant torus, in particular its stability and its reducibility to Floquet form. The second goal is to explore the case of *large* b, to see which kind of interesting phenomena occur.

Remark. If required, we can extend (3) as a Hamiltonian system with phase space $\mathbb{T}^2 \times \mathbb{R}^2 \times \mathbb{R}^2 = \{\theta, J, (x, y)\}$, where J is canonically conjugate to θ. Indeed, if we take as a Hamiltonian $H(x, y, \theta, J) = \frac{1}{2}y^2 + \omega J + \frac{1}{2}(a^2 + bP(\theta))x^2$, the system reads

$$\dot{\theta} = \omega, \quad \dot{J} = -\frac{b}{2}\frac{\partial P}{\partial \theta}x^2, \quad \dot{x} = y, \quad \dot{y} = -(a^2 + b\,P(\theta))\,x.$$

1.2 Problems and results

1.2.1 Resonance tongues

First we review some relevant elements of the classical theory on Hill's and Mathieu's equation with a *periodic* forcing. Indeed, Hill's equation (1) where the forcing term p is periodic in time, has been widely studied in the literature, compare, e.g., [5, 6] and references given there. For related work on nonlinear parametric forcing see, e.g., [2, 7]. In that case in the (a, b)–plane, infinitely many tongues emanate from the *resonance* points $(a, b) = (\frac{k}{2}, 0)$, $k \in \mathbb{N}$, where these tongues have more or less sharp 'tips'. Outside each tongue the trivial 2π–periodic solution $\mathbb{T}^1 \times \{(0,0)\}$, given by $x = y = 0$, is stable. The classical periodic case of the Mathieu–equation occurs for (1) when $p(t) = \cos(t)$. In this case the k–th resonance tongue has a tip with a sharpness of order $(k-1)$. Notice that in the periodic case, the set of resonances is discrete. Figure 1 displays the resonance tongues for the classical periodic case.

In the present *quasi–periodic* case (1) with p given by (2), something similar may be expected regarding the invariant 2–torus $\mathbb{T}^2 \times \{0\}$ of the vector field (3). In this case, the set of resonances

$$(a, b) = (\frac{1}{2}(k_1 + k_2\gamma), 0), \ (k_1, k_2) \in \mathbb{Z}^2,$$

densely fills the a–axis. One may well ask whether 'nearby' resonances emit tongues which 'interfere' for small values of $|b|$ or whether these are separate up to moderate values of b. Figure 2 displays the resonance tongues in the case where p is given by (2), with the golden mean ratio of frequencies.

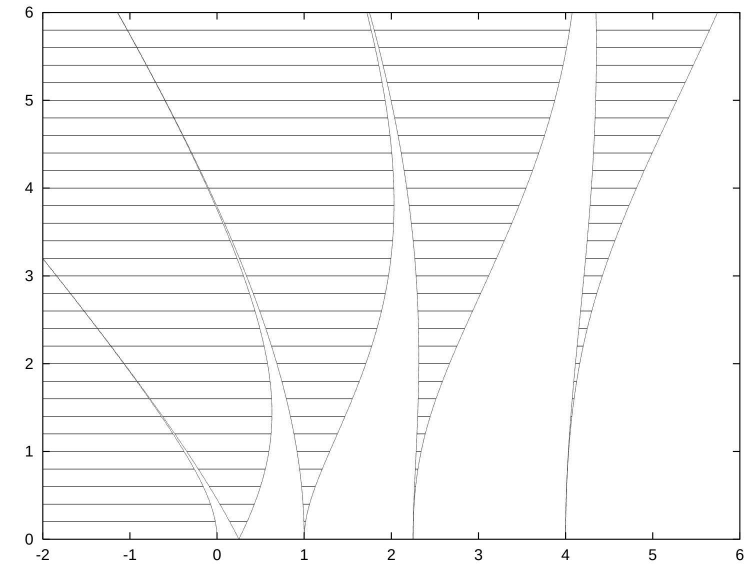

Figure 1: Tongues of the classical Mathieu equation in the (a^2, b)–plane.

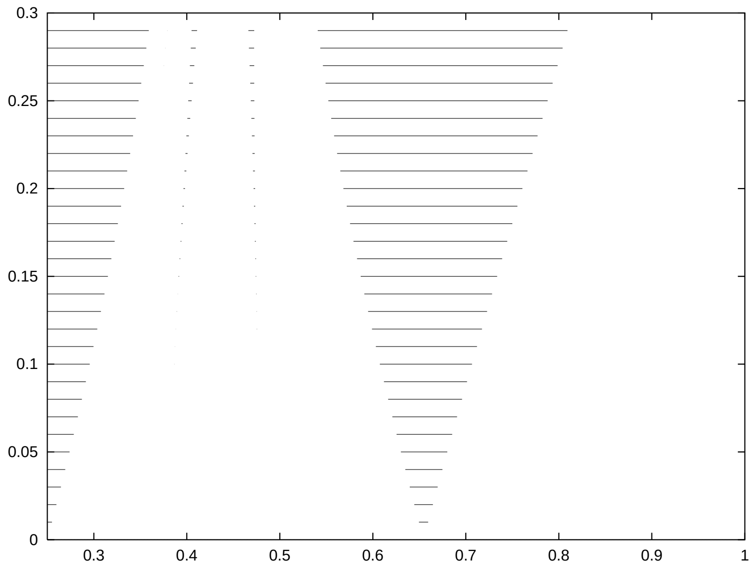

Figure 2: Main tongues, drawn in the (a^2, b)–plane, of Hill's equation with quasi–periodic forcing $p(t) = \cos t + \cos(\gamma t)$.

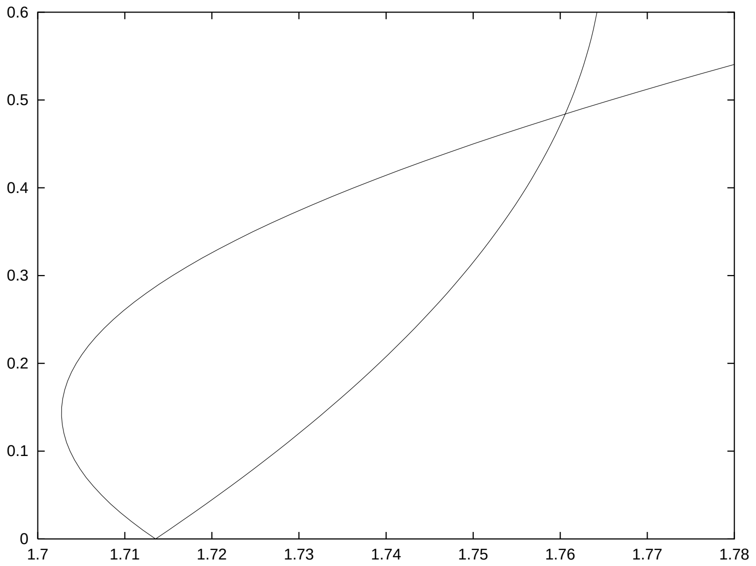

Figure 3: Instability pocket in the (a^2, b)–plane, of Hill's equation with quasi–periodic forcing $p(t) = \cos t + \cos(\gamma t) + 0.3\ \cos((1 + \gamma)t)$.

1.2.2 Instability pockets

Another interesting phenomenon concerns *instability pockets*. In the periodic case these occur in perturbations of the classical Mathieu cases like $p(t) = \cos(t) + c\ \cos(2t)$, where c is a small parameter. Indeed, the boundaries of the second resonance tongue, emanating from $(a, b) = (1, 0)$, cross at an asymptotic distance of the order of $|c|$ from the a–axis, thereby creating an instability pocket. In [5, 6] this phenomenon is qualitatively explained by singularity theory. Presently, an analogue of such a perturbation is given by the following modification of equation (2):

$$p(t) = \cos(t) + \cos(\gamma t) + c\ \cos((k_1 + k_2\gamma)t), \tag{4}$$

for fixed integers k_1, k_2 and with c another small parameter.

Let us give a rough computative argument for the occurrence of instability pockets. The resonance tongue with tip at $(a, b) = (\frac{1}{2}(k_1 + k_2\gamma), 0)$ has two boundaries that can be accurately approximated by an averaging or normalizing procedure, which provides $a - \frac{1}{2}(k_1 + k_2\gamma)$ as a power series in b. In the normal form, each stability boundary is built up from two types of contribution, one type generated by the term $b\,(\cos(t)+\cos(\gamma t))$ and the other by $bc\ \cos((k_1+k_2\gamma)t)$. Also terms showing up as combination of both perturbations can play an important role. All these types of contribution can have dominant terms depending on c and on various powers of b. Hence they 'cancel' for some small values of b, thereby creating instability pockets. This is similar to what happens in the periodic case, see [5, 6]. Figure 3 displays an instability pocket, for p as in (4), where $k_1 = 1, k_2 = 1$ and $c = 0.3$. Later on we return to the analysis of these tongues based on normal forms.

1.2.3 Further problems, a numerical investigation

The linear equation (1) yields the normal linear part of the invariant 2–torus $\mathbb{T}^2 \times \{0\}$. We say that (1) or, equivalently (3), is *reducible* (to Floquet form) if it can be reduced to constant coefficients by means of a linear change of the variables x and y, depending quasi–periodically on time. In the periodic case, the classical Floquet theory solves this problem. In the quasi–periodic case reducibility is not always possible. Several results concerning nonreducibiltiy in similar or wider contexts can be found in [22, 10, 11], [15], [17, 18], [19] and [3, 4, 8, 9].

For larger values of $|b|$ the perturbative method is less effective and we resort to a numerical exploration. Good tools for such a study of equation (1), or system (3), for any value of the parameters (a, b) are the maximal Lyapunov exponent and the rotation number. To this end we introduce an algorithmic approach, which proves very useful in practice.

First we reformulate the problem as follows. In the periodic case all information concerning the properties of (1) is contained in the monodromy matrix, i.e., the fundamental matrix which starts at the identity for $t = 0$ evaluated at $t = T$, T being the period of p. Equivalently we can use the Floquet matrix, i.e., the logarithm of the monodromy matrix divided by T. Compare, e.g., [5, 6].

In the present case of (2) with two angles θ_1, θ_2 and the corresponding frequencies $\omega_1 = 1$ and $\omega_2 = \gamma$, we select one (e.g., θ_1 with period 2π.) But then the angle θ_2 will take the succesive values $\{2n\pi\gamma \mod 2\pi\}, n \in \mathbb{N}$. Therefore, the 'monodromy' matrix also depends on the value of θ_2 at the beginning of each time interval. Let $M(\theta)$ be the fundamental matrix of (1) with $p(t) = \cos(t) + \cos(\theta + \gamma t)$, starting at the identity matrix at $t = 0$ and evaluated at $t = 2\pi$. Next we define a sequence $\{P_n\}$ of matrices, using the skew product transformation:

$$(P, \theta) \mapsto (M(\theta)P, \theta + 2\pi\gamma \mod 2\pi) \tag{5}$$

starting at $(P, \theta) = (I, 0)$. So $P_n(\theta) = M(\theta)P_{n-1}(\theta)$, $n \in \mathbb{N}$, where all matrices $P_n(\theta)$ are symplectic. Note that in the periodic case $P_n = P^n$ for the linear Poincaré map P.

We are interested in the 'average' properties of this sequence. We study (the existence of) a limiting behavior both in the 'expanding' and in the 'rotating' properties. Let μ_n be the dominant eigenvalue of P_n. Then the *maximal Lyapunov exponent* is defined by

$$\lambda = \lim_{n\to\infty} \frac{1}{n} \log |\mu_n|, \tag{6}$$

which happens to be independent of the initial value of θ. Similarly we consider the rotation associated to P_n. Here one has to consider the rotation on the lift, that is, without taking $\mod 2\pi$. To do an effective computation it is enough to start with any normalized vector (e.g., $(1, 0)$) and then to study the arguments of the successive vectors obtained by applying the matrix $M(2n\pi\gamma \mod 2\pi)$ to the previous case. Let α_n be the successive values obtained for the arguments (in the lift; this requires some knowledge of the effect of the successive M matrices on vectors). Then the *rotation number* is defined as

$$\rho = \lim_{n \to \infty} \frac{1}{n} \alpha_n, \tag{7}$$

independent of the initial value of θ.

Remarks.

1. We give some hints on the effective computations, just describing the methods used for a rough exploration. See the Appendix for concrete details and further refinements.

   One possible approach is to do the computations by just integrating (1) over a long time span (say, up to $t = 2\pi \times 10^5$ or $t = 2\pi \times 10^6$). However, this is time consuming and moreover can be severely affected by the propagation of errors. Therefore both more efficiency and accuracy are required.

2. Since we need to know many matrices $M(\theta)$, we used the expeditive way to compute these for an equally spaced mesh of θ–values in $[0, 2\pi)$. Then the values for other θ are found by interpolation. Typically the number of points and the order of the polynomial interpolation range from 200 to 1000 and from 7 to 15, respectively, again in what concerns rough explorations.

3. The computation of each of the $M(\theta)$, for the selected equispaced set of θ–values, is carried out accurately and fast by using a Taylor series method. This method requires the computation of higher order derivatives of x. Starting with x and $\dot{x}$ the value of $\ddot{x}$ is available from (1). Higher order derivatives are obtained by applying the Leibnitz rule to (1). An optimal choice of the order of the expansion and of the stepsize is required. A typical 'optimal' order ranges from 20 to 30.

4. Proceeding as described one can rapidly obtain up to 10^6 iterates. Nevertheless we applied a 'test of goodness' to our estimates of both λ and ρ. Assume that we produce estimates of these every $10,000$ iterates, skipping a transient of, say, $30,000$ iterates. Then we can compare the estimated values of Lyapunov exponent and rotation number. If three consecutive estimates (for instance, after, say $130,000$, $140,000$ and $150,000$ iterates) agree within a prescribed tolerance, the estimate is considered as sufficiently good. Typical tolerances range from 10^{-5} to 10^{-7}. Furthermore the scannings usually are done not allowing very large changes in λ or ρ from one value of a to the next, in order to not to miss interesting phenomena. Here, the stepsize in a is reduced to 10^{-9} if needed.

The first theoretical problem then is the existence of these two numbers. It is clear that, if (1) is reducible, then the corresponding Floquet matrix and the reducing matrix–transformation immediately supply us with the existence. For small b the set of a–values with an instable 2–torus has a rotation number in the set

$$\mathcal{R} = \left\{ \frac{1}{2}(k_1 + k_2\gamma) \in \mathbb{R} \mid k_1, k_2 \in \mathbb{Z} \right\},$$

exactly corresponding to a resonance tongue, by definition. Now fix b small and consider varying a. Despite the fact that the set of intersections with the tongues is dense, the measure of its complement is still relatively large, as proved in [17], for instance. More concretely, the set of values of a for which reducibility is not possible is exponentially small in b, under generic conditions. In fact the result is even sharper, since in [17] only reducibility to the stable or 'elliptic' case is considered. Hence, the resonant zones are thrown out. But it is well known that in the hyperbolic case reducibility is always possible. These results fit, once more, inside KAM–theory.

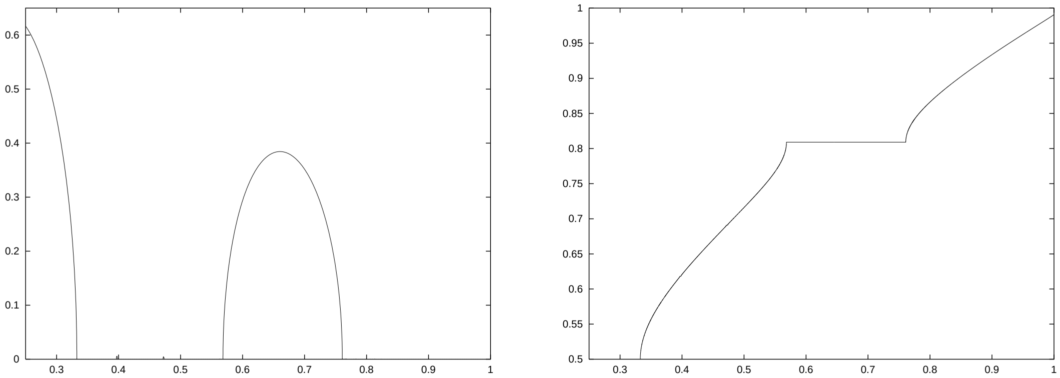

Maximal Lyapunov exponent λ Rotation number ρ

Figure 4: Plots of Lyapunov exponent and rotation number for $b = 0.2$.

Keeping b small, a large part of a–values taken in any simulation scanning a segment, should correspond to points outside the resonance tongues. Indeed, the estimated values of λ do not significantly differ from zero. This can be seen in figure 4 where for b as large as $b = 0.2$ we plot, to the left, the estimated Lyapunov exponent as a function of a^2 in the range $[0.25, 1]$. The right hand figure shows the corresponding value of the rotation number in the same range. Only the resonances associated to $(k_1, k_2) = (1, 0)$ and to $(0, 1)$ are relevant in the left and central parts of this range. Very small spikes associated to the resonances $(-2, 2)$ and $(3, -1)$ start to show up for a^2 close to 0.382 and 0.477, respectively. It is clearly seen that the Lyapunov exponent is only positive in the resonance tongues, that is, when the couple (a, b) is inside $\mathcal{R}$. Apart from the 'large' steps seen in the rotation number plot, there is a countable set of steps (every time ρ takes a value in $\mathbb{Q}$) but they are hardly visible. In the complement of $\mathcal{R}$ the value of λ is zero.

Note also that from [16] it follows that, given some interval in the a–variable, some 'almost' reducibility is possible, uniformly in a. More concretely, equation (1) can be reduced to constant coefficients except by a remainder which is, at most, exponentially small in b.

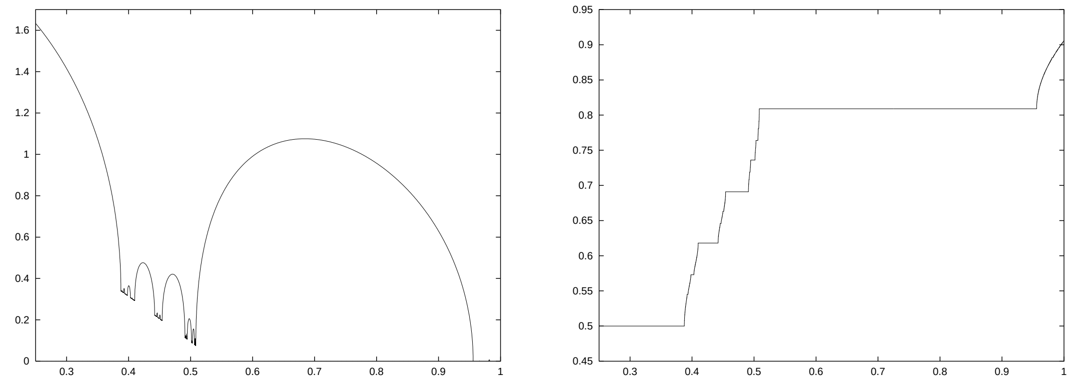

Maximal Lyapunov exponent λ Rotation number ρ

Figure 5: Plots of Lyapunov exponent and rotation number for $b = 0.6$.

On the other hand, for larger values of b (for the present choice of p this starts to occur for b–values around 0.5) and for $a \in [0.5, 1]$ we can still speak of 'resonance tongues'. Here the rotation number belongs to $\mathcal{R}$, but it is no longer true that the points outside these tongues have $\lambda = 0$. Figure 5 displays the same data as figure 4 but for $b = 0.6$. There many more steps are seen and, furthermore, outside the steps the Lyapunov number is definitely different from zero. See figures 6 and 7 for magnifications of small a ranges and nearby values of b, and section 5 for many additional details.

We observe that for (a, b)–values outside the tongues with $\lambda > 0$ evidently reduction to Floquet form is impossible, since in a 2×2–matrix it is impossible to incorporate $\pm\lambda$, $\pm\rho$.

An interesting global phenomenon concerns the line $\mathcal{C}$ in the (a, b)–plane, see figures 9 and 10. Here a 'collapse of resonances' seems to occur. Moreover, for fixed b, on the left–hand side of this line parameter–points outside the tongues seem to have positive λ. See section 5 for a numerical investigation on the origin of the collapse. Also see the Conclusions for a summary.

2 Resonance tongues

Fixing the integers k_1 and k_2, we now study a neighbourhood of the resonance $(a_0, b) = (\frac{1}{2}(k_1 + k_2\gamma), 0)$.

Definition 1 *The resonance tongue associated to the tip $(a_0, 0)$ is defined as the subset of the (a, b)–plane, where the rotation number $\rho(a, b)$ exists and equals $\frac{1}{2}(k_1 + \gamma k_2)$.*

The problem is that for given small b, the set of a–values contained in the union of all tongues is dense.

In this context we slightly change the notation of (1), first setting $a^2 = a_0^2 + \alpha_0$. The standard scalings

$$x = \frac{\xi}{\sqrt{a_0}},\ y = \eta\sqrt{a_0}$$

and the passage to complex coordinates

$$\xi = \frac{q+ip}{\sqrt{2}},\ \eta = \frac{iq+p}{\sqrt{2},}$$

allow us to express the Hamiltonian of (3) as follows:

$$H = a_0 iqp + \frac{q^2 - p^2 + 2iqp}{2}\left(\frac{\alpha_0}{2a_0} + \frac{b}{4a_0}(\cos t + \cos(\gamma t))\right), \tag{8}$$

compare [6]. Let J be a variable canonically conjugate to the time t and let us abbreviate $z_1 = \exp(it)$, $z_2 = \exp(i\gamma t)$. Then (8) can be written as an integrable part, H_0, and a perturbation, H_1, given by

$$\begin{aligned} H_0 &= J + a_0 iqp, \\ H_1 &= \hat{b}(q^2 - p^2 + 2iqp)(\hat{\alpha}_0 + z_1 + z_1^{-1} + z_2 + z_2^{-1}), \end{aligned} \tag{9}$$

where

$$\hat{\alpha}_0 = \frac{2\alpha_0}{b},\ \hat{b} = \frac{b}{8a_0}.$$

We can follow the Giorgilli–Galgani algorithm [13], for instance, to carry out the normalization (averaging). For similar considerations in the periodic case see [6]. Starting with $H_{0,0} = H_0$ and $H_{1,0} = H_1$, we compute recurrently

$$H_{j,k} = \sum_{n=1}^{k} \frac{n}{k}[G_n, H_{j,k-n}],\ j = 0, 1,\ k > 0,$$

where $[\, ,]$ denotes the Poisson bracket. The functions G_n are determined to cancel the time dependence, as far as possible. The transformed Hamiltonian then is $K = K_0 + K_1 + K_2 + \ldots$, where $K_0 = H_{0,0}$ and $K_n = H_{1,n-1} + H_{0,n}$. Note that the 'order' of a term can be considered to be the order with respect to the auxiliar parameter $\hat{b}$. Therefore, K_n contains $\hat{b}^n$ as a factor.

It is easy to check that the action of $H_{0,0}$ on $q^r p^{-r} z^k$, where $z^k = z_1^{k_1} z_2^{k_2}$, by means of the Poisson bracket is

$$[H_{0,0}, q^r p^{-r} z^k] = q^r p^{-r} z^k i(a(2-2r) - (k_1 + \gamma k_2)),$$

showing that all terms with $a(2-2r) - (k_1 + \gamma k_2)$ different from zero (or, at least, not too small) can be cancelled. If a_0 is selected to be $k_1^* + \gamma k_2^*$, (where k_1^* and k_2^* are assumed to be half integers) then the choice $k_1 = \pm 2k_1^*$, $k_2 = \pm 2k_2^*$ produces a resonance (the plus–sign being used for $r = 0$ and the minus–sign for $r = 2$).

This procedure can be implemented automatically. It is immediate to check by induction that if $j + k = m$ then the $H_{j,k}$ are of the form

$$H_{j,k} = q^2 c_1 - p^2 c_2 + iqp(c_3 + c_4),$$

and the corresponding G_m are of the form

$$G_m = i(q^2 c_1 + p^2 c_2) + qp(c_3 - c_4),$$

where c_1 contains terms with real coefficients of the form $\hat{\alpha}_0^{m-s} z^k$ with $|k| = |k_1| + |k_2| = r$ and s and r have the same parity. The terms in c_2 are exactly the same as in c_1 except for a replacement of z^k by z^{-k}. The expression of c_3 is similar to that of c_1, but all terms either have $k_1 > 0$ or $k_1 = 0$, $k_2 \geq 0$. Finally c_4 again is identical to c_3 but for the replacing of z^k by z^{-k}.

Collecting all the terms which appear in the normalization process we reduce the Hamiltonian as follows. For a completely similar procedure see [6].

Theorem 2 (Complex normal form) *Fixing $a_0 = \frac{1}{2}(k_1 + \gamma k_2)$ as before, by a canonical change of coordinates the Hamiltonian $H = H_0 + H_1$, up to an additive remainder, can be reduced to the normal form*

$$\mathrm{NF} = J + a_0 iqp + \mathrm{coef}_1 iqp + \mathrm{coef}_2 (q^2 z^{-k} - p^2 z^k),$$

where, for $|k| = |k_1| + |k_2|$,

- $\mathrm{coef}_1 = \hat{\alpha}_0 + r_1$, *where r_1 is a (real) function depending on $(\hat{b}, \hat{\alpha}_0)$ and containing some power of $\hat{b}$ as a factor,*

- $\mathrm{coef}_2 = \hat{b}^{|k|} \times r_2$, *where r_2 is a (real) function depending on $(\hat{b}, \hat{\alpha}_0)$, but with $r_2(0, 0) \neq 0$.*

- *The order of the remainder is greater than $|k|$ in $\hat{b}$.*

If we skip the remainder and pass to co–rotating coordinates (u, v) defined by

$$u = q \exp(-a_0 it), \quad v = p \exp(a_0 it)$$

we obtain the system

$$\begin{aligned} \dot{u} &= \quad i\,\mathrm{coef}_1\, u - 2\,\mathrm{coef}_2\, v, \\ \dot{v} &= -2\,\mathrm{coef}_2\, u - i\,\mathrm{coef}_1\, v. \end{aligned} \tag{10}$$

Summarizing, formally everything looks exactly like in the periodic case, e.g., see [6]. At the tongue–tip the boundary curves have order of contact $|k|$. The Floquet matrix is given by (10). It also follows that the expression $D = \mathrm{coef}_1^2 - 4\mathrm{coef}_2^2$ determines the stability: $D > 0$ is the stable case and $D < 0$ the unstable one. The boundaries are given by the equation $\mathrm{coef}_1 = \pm 2\mathrm{coef}_2$. This approach also shows that, if the normal form procedure can be made convergent in this way, then for $D < 0$ one has $\lambda = 2\pi\sqrt{-D}$ and $\rho = \frac{1}{2}(k_1 + \gamma k_2)$, while for $D > 0$ one has $\lambda = 0$.

The following conjecture suits with the numerical simulations made up to now. In future research we plan to investigate this further, based on small divisor estimates, and possibly involving resonances and bifurcations, compare [1, 22, 10, 17, 18, 23].

Conjecture 3 *Select any range of a–values (e.g. $a \in [1/2, 1]$). Then, there exists a value $b_0 > 0$ such that for $|b| < b_0$ all tongues are separated by areas where the Lyapunov exponent equals zero.*

3 Instability pockets

We fix the form of p as in (4), taking $p(t) = \cos(t) + \cos(\gamma t) + c\,\cos((k_1 + k_2\gamma)t)$. Then the normal form computation is as before, but the main difference comes from an additional term in coef_2 of the form $c\hat{b}$ times some nonzero number. The tongue boundary again is given by the equation $D = 0$. For a given value of c (with the suitable sign when $|k|$ is odd) we find a zero of D for some small b. This is the 'upper end' of the pocket if $b > 0$, the 'lower end' being at 0. For $b < 0$ the situation reverses. Figure 3 illustrates this phenomenon. By increasing c the upper end of the pocket goes up. Values up to $c = 0.5$ have been tested with success. Larger values interfere with the 'collapse of resonances', described in the next section.

The addition of more parameters with different harmonics, i.e., replacing the term in c in (4) by $\sum_{j=1}^{m} c_j \cos(k_{1,j}\theta_1 + k_{2,j}\theta_2)$, also can be studied by means of the normal form. Looking at a particular resonance one finally obtains a polynomial in the variables b, c_j, $j = 1, \ldots, m$. By a suitable selection of the values of the c_j one can produce zeros of the function D, which give the intersection points associated to the instability pockets. As in [6], for any (small) value of b, this number of zeros (including the one at $b = 0$) can reach the multiplicity $|k|$ of the resonance.

4 Global properties

In this section we present some numerical results which appear for relatively large values of the parameter b.

4.1 Near the tongue boundaries

Near a tongue boundary the Lyapunov exponent and the rotation number seem to behave always as in the case of small b, according to a normal form.

Concerning the Lyapunov exponent: Inside a tongue, when a approaches the boundary of the tongue, $|\lambda(a) - \lambda(a^*)|$ behaves as the square root of $|a - a^*|$, where a^* denotes the corresponding endpoint (left or right) of the interval. For b small $\lambda(a^*)$ is 0. But the behavior looks like $c_L\sqrt{|a - a^*|}$ even for large values of b, where one has $\lambda(a^*) > 0$.

By definition ρ is constant inside the tongue. Let a^* be the left endpoint. Then $\rho(a^*) - \rho(a) \sim c_R\sqrt{a^* - a}$ for $a < a^*$. If a^* is the right endpoint, then $\rho(a) - \rho(a^*) \sim c_R\sqrt{a - a^*}$ for $a > a^*$.

Furthermore, the relation between the constants, c_L and c_R, concerning λ and ρ, respectively, suits the theoretic predictions obtained when normal forms provide sufficiently good approximations.

Some magnifications are shown in figure 6.

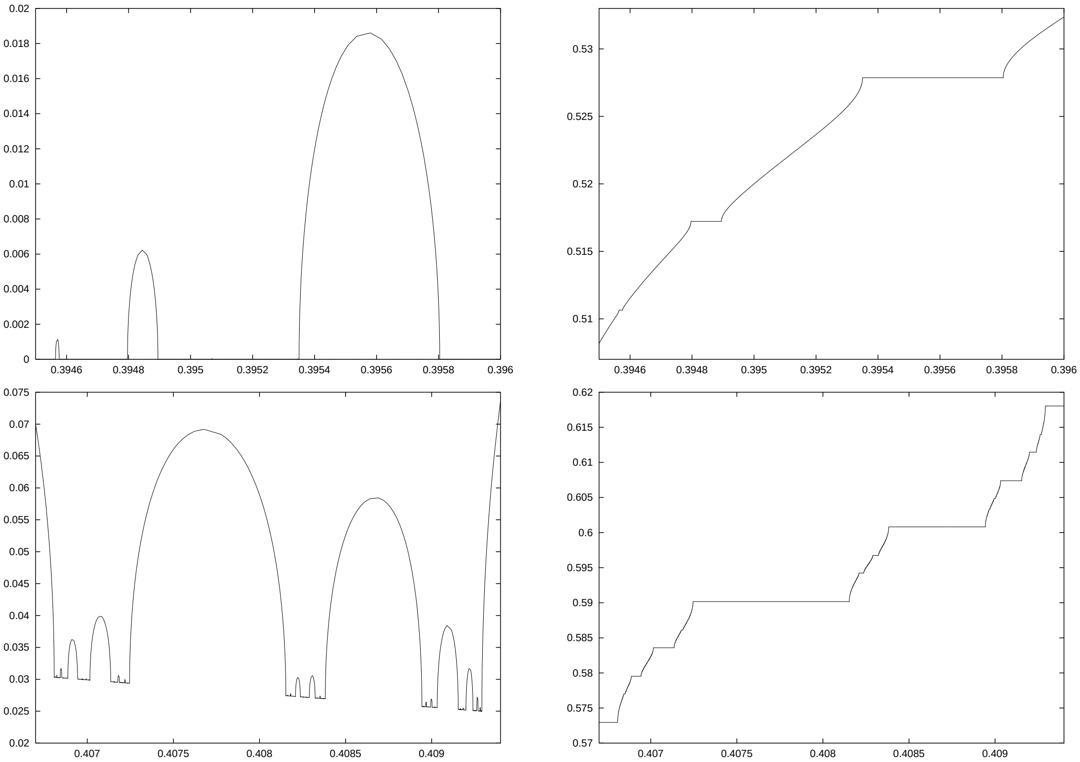

Figure 6: Plots of λ and ρ near the boundary of a tongue. The plots on the left display λ. In the upper case, $\lambda = 0$ outside the tongue and is positive inside. In the lower case we show a situation where outside the tongue λ is still positive. The plots on the right show the corresponding values of ρ, where the square root behavior is clearly seen. The upper plots correspond to $b = 0.5$ and to the a^2–range $[0.3945, 0.396]$. The lower ones to $b = 0.54$ and to the a^2–range $[0.4067 : 0.4094]$.

4.2 The collapse of resonances

A puzzling phenomenon is the 'collapse' of resonances. When the parameter b is increased, the boundaries of different tongues approach. After this, the Lyapunov exponent is no longer zero outside the resonance tongues, but positive. Also the variation of ρ as a function of a seems to be much sharper than just the effect of a square root. Figure 7 shows λ and ρ for $b = 0.51$, 0.54, 0.57 and 0.60. This effect is specially remarkable for a range of a^2 between 0.38 and 0.52.

A refined computation allows to detect and measure the width (width $= a_{\text{right end}} - a_{\text{left end}}$) of all the tongues of width greater than 10^{-7}, for a set of values of b. A plot of the measure of the complement of the resonance tongues as a function of b is given in figure 8. The a^2–domain of our consideration is $[0.35, 0.75]$. The measure of the complement depends, of course, on the selected domain of a. For shorter domains the measure of the complement shrinks to values very close to zero for b–values for which the line of collapse of resonances is crossed.

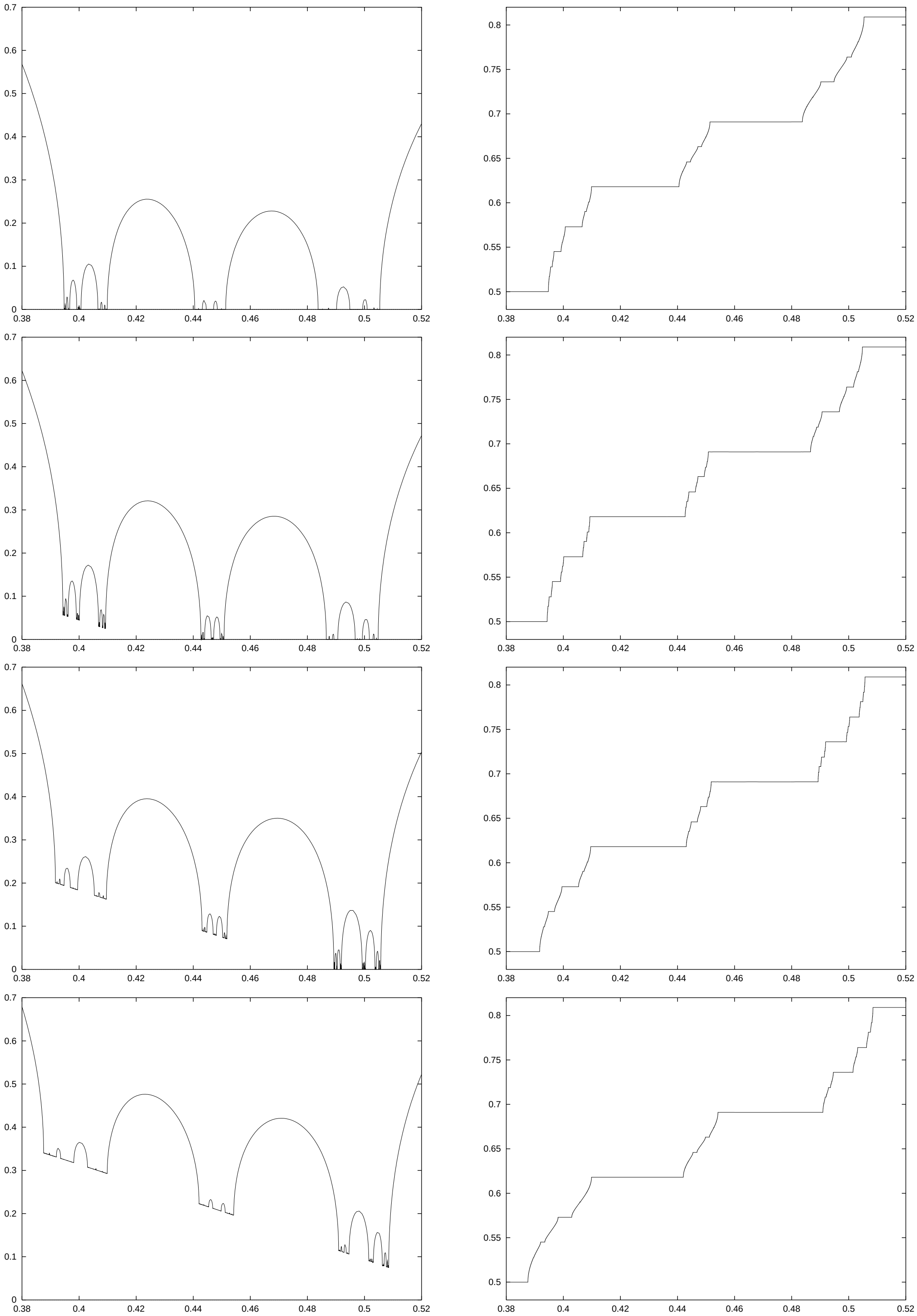

Figure 7: Plots of Lyapunov exponent λ (left hand figures) and rotation number ρ (right hand figures) for $b = 0.51$, 0.54, 0.57 and 0.60 (from top to bottom).

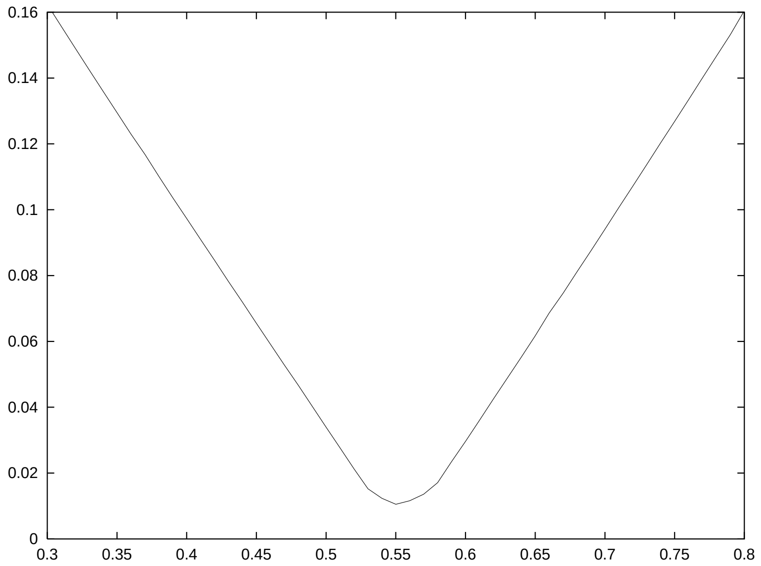

Figure 8: Estimate of the measure of the complement of the set of resonances as a function of b.

Regarding the Lyapunov exponent, we also observe the following. Outside the 'bumps' associated to the tongues, λ as a function of a^2, for b–values where it is positive, seems to lie on a straight line. This line intersects $\lambda = 0$ for some value of a depending on the current b–value. In fact, this may well be a proper definition of the *collapse line*. For (a, b)–values at the left upper part of this line, the Lyapunov exponent seems to be positive even outside the resonance tongues, while below it seems to be zero outside the tongues. Figure 9 displays a general view of the resonance tongues and an estimate of the position of the collapse line for $a^2 \in [0.25, 1]$ and $b \in [0, 1]$. Figure 10 shows a magnification for $a^2 \in [0.3916, 0.4104]$ and $b \in [0.5, 0.57]$. All resonances of order less than or equal to 101 in this a–range are displayed. From left to right these are (including the large resonance zones which start to be seen at both left and the extrema): $(1, 0)$, $(-54, 34)$, $(35, -21)$, $(-20, 13)$, $(14, -8)$, $(-41, 26)$, $(48, -29)$, $(-7, 5)$, $(-62, 39)$, $(27, -16)$, $(-28, 18)$, $(61, -37)$, $(6, -3)$, $(-49, 31)$, $(40, -24)$, $(-15, 10)$, $(19, -11)$, $(-36, 23)$, $(53, -32)$, $(-2, 2)$.

We end this section with two further observations. The first is that the resonance tongues become narrower when b is increased with respect to the collapse line. Secondly, the width of the resonances for small b follows the rule given by the order of the resonance. If we compare one resonance to another, it seems that they decay in an exponential way with respect to the order. Then, the coefficients c_L in the square root law or the maxima of the bumps in the λ follow similar rules.

This is no longer true near the collapse. Indeed, in that case it seems that the width of the resonances is like 1/(some power of the order of the resonance), this power decreasing near 2 when we approach a collapse. See the next section for more accurate data and the related figures, and to see how a more detailed numerical study reveals additional interesting characteristics.

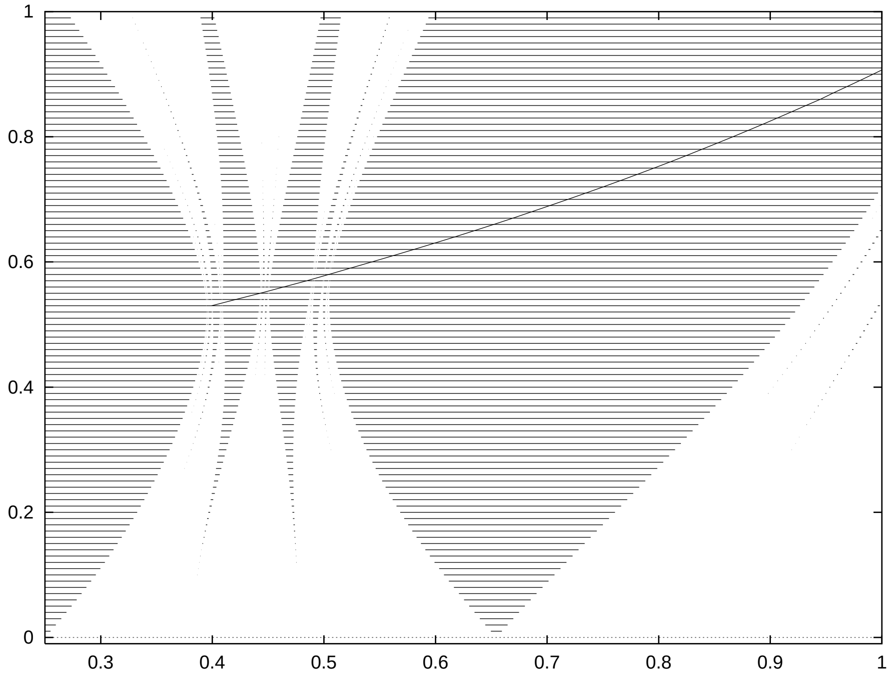

Figure 9: Resonance zones and collapse line.

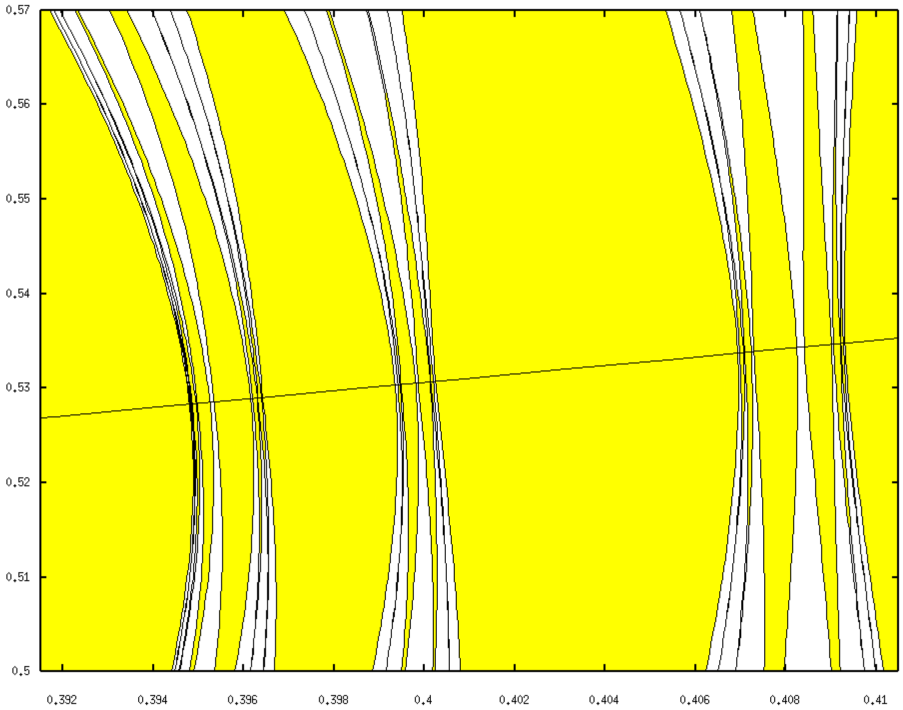

Figure 10: Magnification of the previous figure

5 A detailed numerical study

The phenomena near the collapse line of resonances ask for explanation. In this section we present a detailed description of the phenomenology. Trying to make the presentation clear we give here results concerning three different aspects: The phase space after skipping the eventual instability, the Fourier space and the properties of λ and ρ. We refer to the Appendix for all the computational details.

5.1 On the phase space. Skipping instability

Consider first a case where $\lambda = 0$ and where ρ is non resonant. We study the behavior of the iterates as a function of the number of the iteration, or – to put it more geometrically –, at the set made of the first column of the matrices P_n (see after (5)) after a transient. We select $(a^2, b) = (0.408, 0.4)$. The results are displayed in figure 11 1). They show a clear quasiperiodic behavior corresponding to the projection of a 2–torus. Indeed, we have 3 basic frequencies: $1, \gamma$ and ρ. Since we study iterates at t–values that are multiples of 2π, we skip the frequency 1, but γ and ρ remain. It the present case $\rho \sim 0.6032880958$. The probability of picking ρ such that $(1, \gamma, \rho)$ satisfies a diophantine condition is 1.

To display cases for which $\lambda > 0$ we first have to skip the instability. This is achieved by introducing the matrices $\hat{P}_n = \exp(-n\lambda)P_n$, where the estimated value of λ is used and n is taken after a transient. We shall refer to $\hat{P}_n$ as the *scaled matrices*. Again in figure 11 we display in 2) the result for $(a^2, b) = (0.413, 0.4)$ which shows an invariant curve (section of a 2–torus) and in 3) and 4), respectively, the results for $b = 0.6$ and the values $a^2 = 0.408$ (nonresonance) and $a^2 = 0.413$ (resonance). In 4) the behavior is similar to 2), except for the fact that the invariant curve is more 'wild' and do not projects as a simple closed curve. However, the case 3) displays an ugly set of points, far away from quasiperiodicity. We have limited the window to better show the central part. Other points fall far away from the 'central region'. The parameters for which $b = 0.4$ are below the line of collapse of resonances, while the ones with $b = 0.6$ are above that line.

It is also instructive to look at data corresponding to the nonresonant case above the collapse line. Indeed, there are several clear peaks. To make this more evident we plot the quantity $\Sigma_{i,j=1,2}\left(\hat{P}_n\right)^2_{i,j}$ for a large range of iterates. The peaks appearing in figure 12 with an amplitude larger than 0.6×10^9 are located at values of n (skipping the transient) equal to 78306, 78683, 153708 and 200076. All the differences (377, 75025 and 46368) are Fibonacci numbers. The same is true if we also consider peaks above a lower threshold, with the eventual inclusion of differences which are the sum or the difference of two relatively large, but non consecutive, Fibonacci numbers. For instance, the closest peak larger than 10^8 after the largest one in the plot occurs with $\Delta n = 70844 = 75025 - 4181$, a difference of two such numbers. Note that despite this wild behavior of the $\hat{P}_n$ matrices, the $M(\theta)$ matrix is quite regular. In figure 12 we also display the behavior of its components as a function of θ. It seems that some small amplitude high order harmonics of $M(\theta)$ 'do not average well' under composition.

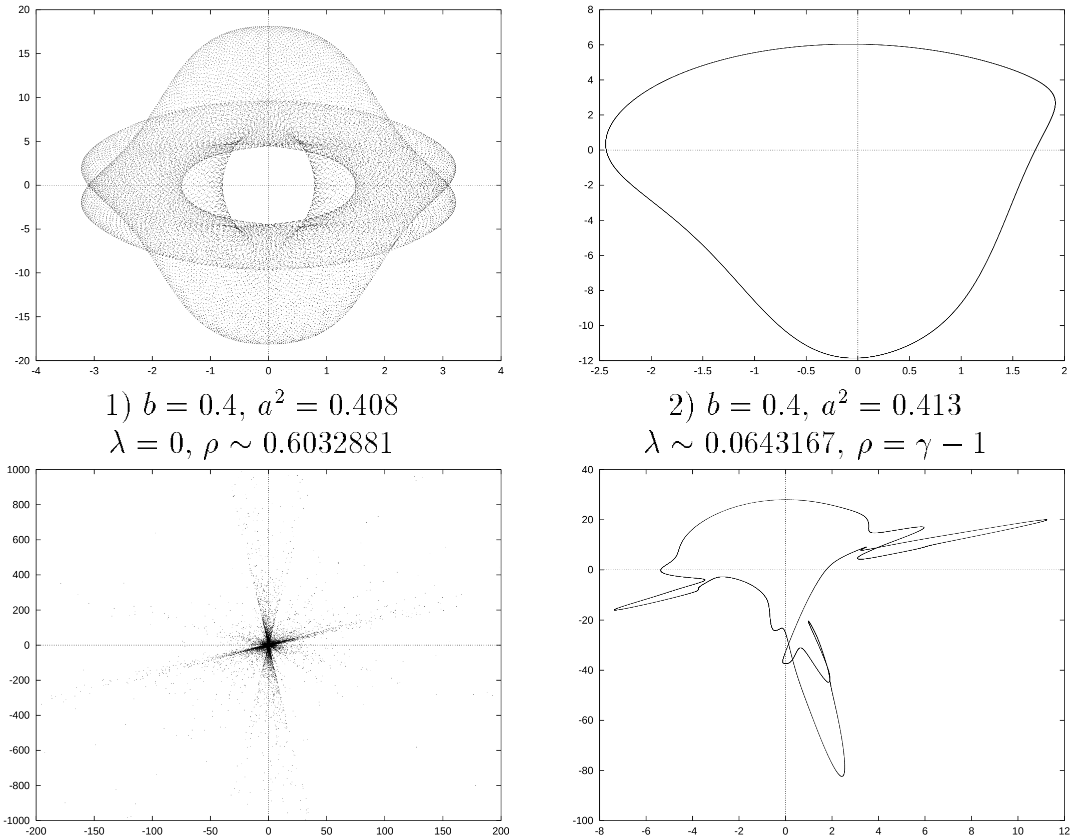

1) $b = 0.4$, $a^2 = 0.408$
$\lambda = 0$, $\rho \sim 0.6032881$

2) $b = 0.4$, $a^2 = 0.413$
$\lambda \sim 0.0643167$, $\rho = \gamma - 1$

3) $b = 0.6$, $a^2 = 0.408$
$\lambda \sim 0.2967086$, $\rho \sim 0.5999420$

4) $b = 0.6$, $a^2 = 0.413$
$\lambda \sim 0.4178172$, $\rho = \gamma - 1$

Figure 11: Plots of iterates of the first column of matrices P_n (case 2) or matrices $\hat{P}_n$ (the remaining cases). In all cases, except in 1), we used 2^{14} iterates after a transient. In case 1) this number is 2^{15}. The transient has a length of 10^6 iterates. The estimated values of λ and ρ are also shown.

5.2 Fourier analysis

To enter deeper into the structure of the data displayed in the previous subsection, we perform a Fourier analysis of the scaled matrices. Figure 13 shows results corresponding to the analysis of an element of the scaled matrices, for each of the couples of parameters displayed in figure 11. The data shown are the norms of the different harmonics for the $(2,1)$–entry as a function of the number of the harmonic. The number of harmonics is 2^{17} and the last one corresponds to a frequency of $\frac{1}{2}$. Note that the frequencies are shown modulo 1 and that a frequency $\nu \in (\frac{1}{2}, 1)$ appears in the place corresponding to $1 - \nu$.

In the case where the system is reducible, the analysis done in this way contains both the frequencies of the change of variables reducing the equation and the 'proper' frequency of the reduced equation. In the resonant case the 'proper' frequency is of the form $(k_1 + k_2\gamma)/2$ for suitable values of k_1 and k_2.

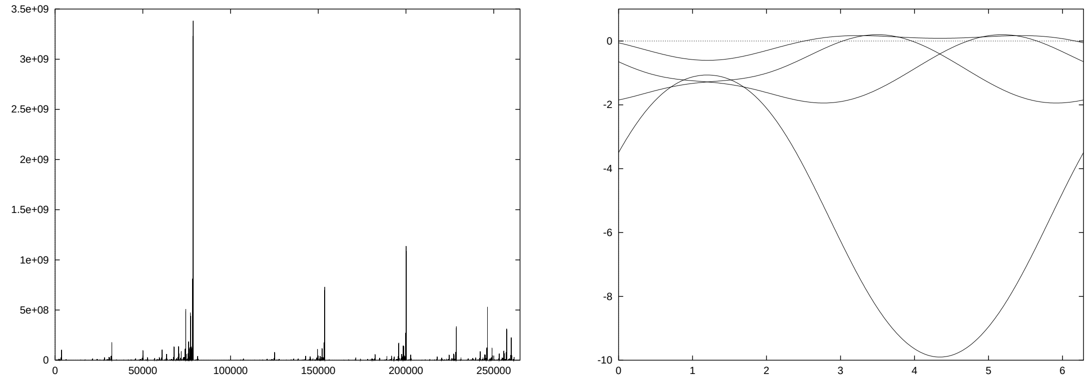

Figure 12: Left: Peaks of the sum of the squares of the elements of the scaled matrix after a transient of 2×10^6 iterates, for the next 2^{18} iterates. Parameters $(a^2, b) = (0.408, 0.6)$. Right: The 'monodromy' matrix as a function of θ for $\theta \in [0, 2\pi]$. For $\theta = 0$ the order, from top to bottom, of the matrix–entries is $(1,2)$, $(1,1)$, $(2,1)$ and $(2,2)$.

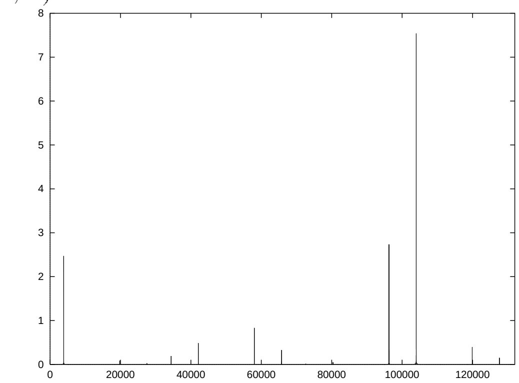

1) $b = 0.4$, $a^2 = 0.408$

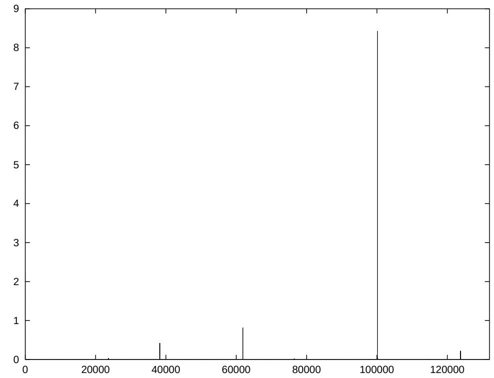

2) $b = 0.4$, $a^2 = 0.413$

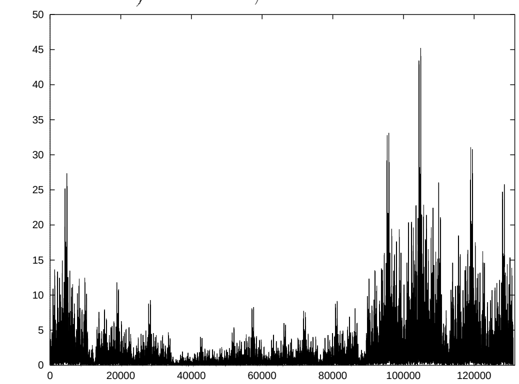

3) $b = 0.6$, $a^2 = 0.408$

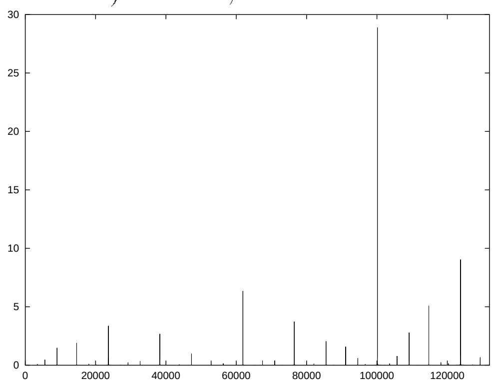

4) $b = 0.6$, $a^2 = 0.413$

Figure 13: Results of the Fourier analysis corresponding to the element $(\hat{P}_n)_{2,1}$ for each of the cases in figure 11. All cases, except 3) show quasiperiodic behavior. Number of data analyzed: 2^{18}.

It is easily seen that the nonresonant cases above the collapse line seem far from quasiperiodic. To have a quantitative measure of this the following computation has been carried out. After doing the Fourier analysis we look for the 'dominant harmonics'. Let $A_{\max}$ the maximum amplitude of the harmonics. Then we set up a 'scale' of the size of the harmonics: A harmonic is said to be 'of order' m if the corresponding amplitude belongs to $[0.8^{m+1}, 0.8^m] \times A_{\max}$, where the value 0.8 has been selected as a suitable choice. Given a Fourier analysis we select a value m^* such that the number of harmonics of order $m \leq m^*$ is at most 100, but the number of harmonics of order $m \leq m^* + 1$ is greater than 100. A large value of m^* means a quick decrease of the size of the harmonics, while a small value denotes a 'rough' function. Figure 14 displays the value of m^* as a function of a for two ranges of a–values and four different values of b. This offers additional evidence for the very different behavior above and below the collapse line.

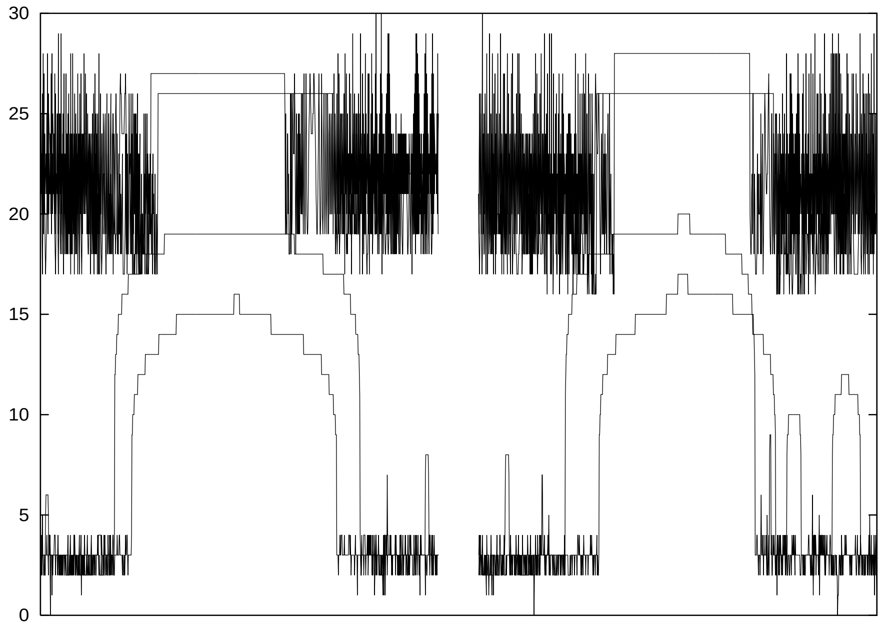

Figure 14: Measure for the 'roughness' of the Fourier analysis of the scaled matrices. Low values denote a rougher behavior. See the text for additional explanation. Approximately the lines, from top to bottom, correspond to $b = 0.2$, 0.4, 0.6, 0.8. For each value of b there are two ranges of values of a^2. They have been selected so that they contain the resonances $(-2, 2)$ and $(3, -1)$ in their interior. These ranges are $[0.395, 0.4]$ and $[0.47, 0.475]$ for $b = 0.2$, $[0.408, 0.430]$ and $[0.455, 0.478]$ for $b = 0.4$, $[0.408, 0.444]$ and $[0.452, 0.494]$ for $b = 0.6$ and $[0.402, 0.427]$ and $[0.473, 0.504]$ for $b = 0.8$. Furthermore, for the last three values of b, some subranges in the middle of the resonances and where m^* is constant, have been suppressed. In each range 1000 values of a were used.

Another interesting feature is the behavior of the dominant harmonic as a function of a for fixed b. Figure 15 displays some typical cases. We have taken the $(2, 1)$

entry of the matrix $\hat{P}_n$. Let $A_{\max}$ the maximum amplitude of the different harmonics, corresponding to some frequency $\nu_{\max}$. With a few exceptions $\nu_{\max} = \rho$. Only in a few cases one has that $\nu_{\max} \neq \rho$, and then $A_{\max}$ is slightly larger than A_ρ for this concret entry of the matrix. Hence, for coherence, we have computed A_ρ as a function of a. In all cases, either below, above or across the collapse line, the behavior is smooth inside the resonances. Going to the endpoints of a resonance there appear two different cases: either the amplitude has a sharp peak at the endpoint or is decreases to very small values. Outside the resonances the behavior is wild if $\lambda > 0$ and only small irregularities appear if $\lambda = 0$. Figure 15 illustrates some details below, across and above the collapse line.

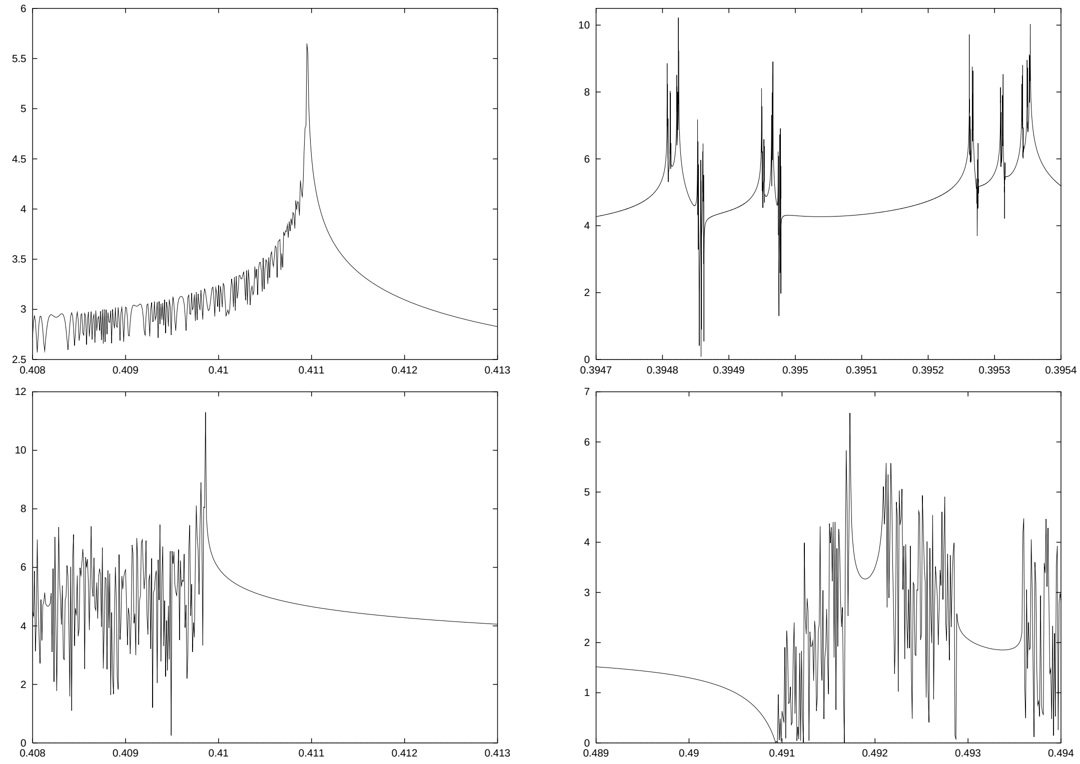

Figure 15: Behavior of the amplitude A_ρ of the harmonic whose frequency coincides with ρ in the Fourier analysis of $(\hat{P}_n)_{(2,1)}$. Upper left: $b = 0.4$, below the collapse line. Upper right: $b = 0.528$, very close to the collapse line. The 'irregularities' are due to the large number of resonances. Lower part: $b = 0.6$, above the collapse line. Large irregularities are seen outside the resonant zones. The stepsize in a^2 is 10^{-5}, except for $b = 0.528$, where 10^{-7} has been used. In order to better visualize small and large components simultaneously, on the vertical axis the variable is $\operatorname{arcsinh}(A_\rho)$ instead of A_ρ.

5.3 The behavior of λ and ρ close to the collapse line

In figure 7 we have seen a sample of estimates of λ and ρ close to the collapse line. Some more details are shown in figure 16, where successive magnifications are done. This figure also gives support to the 'collapsing' effect. The large resonance to the left of these figures is related to the multiplicators $k_1 = 1$, $k_2 = 0$ and, hence, to $\rho = 0.5$. Notice that in the last row of figure 16 the values of b have been selected in such a way that λ starts to be positive outside the resonances.

To locate points in the collapse line we chose the simplest case, looking for the (a, b)–value where the right hand boundary of the $(1, 0)$–resonance intersects with it. Figure 17 shows a plot of λ for $b = 0.5284$ and a range $a^2 \in [0.39479, 0.395]$ such that the first 'contact' of λ with 0 occurs for ρ slightly greater than 1/2. The values of λ outside the resonances seem to be very close to a curve which, in turn, is quite close to a straight line. It is also plotted on the figure. This allows to obtain, by extrapolation, the value of $a = a_c(b)$ at which the 'contact' is produced. Again plotting $\rho(a_c(b), b) - 1/2$ (or some equivalent magnitude) as a function of b (see again figure 17), allows to predict the value of b for which $\rho(a_c(b), b) = \frac{1}{2}$. The value $(a^2, b) \sim (0.39479983, 0.528315)$ is found. A similar process can be used for any resonance.

Having located these values, it is possible to examine the behavior of the resonances. Two items seem to be specially relevant:

- For a given value of b, the maxima–value of the resonance bumps in λ as a function of the value of the associated frequency. Figure 18 displays the results for $b = 0.5284$, showing the heights for frequencies immediately to the right of $\frac{1}{2}$. The range of a is selected so that we are close to the collapse line. We see a clear organization on the structure of this set, the heights behaving almost linearly with respect to some limit frequency. Similar structures are also seen at smaller scales. This occurs at the crossing of the collapse line. For values of the parameters not too close to that line, the secondary bumps are hardly visible.

- For a selected set in $\mathcal{R}$, the related heights of the resonance bumps in λ as a function of b. Figure 19 displays the results. The values of b used here range from 0.528 to 0.53 with stepsize 10^{-4}, plus additional values in $(0.5283, 0.5284)$ with stepsize 10^{-4}. The selected resonances have frequencies ν in $(1/2, (35 - 21\gamma)/2 \sim 0.5106431181)$. The lowest order resonances are $(35, -21)$, $(-54, 34)$, $(90, -55)$, $(-143, 89)$, $(179, -110)$, $(-198, 123)$, $(234, -144)$ and $(-287, 178)$. All these number are (eventually ± 1) equal to Fibonacci numbers or to the sum or difference of two of these. For all values of b in this range all the resonances in the corresponding range of order $|k| = |k_1| + |k_2| < 2000$ have been detected. For the values of b closer to the critical value 0.528315 found before, i.e., for $b = 0.5283$ and $b = 5284$, all resonances in this range with $|k| < 10000$ have been detected. (Some of the well detected resonances have order greater than 50000). These are the

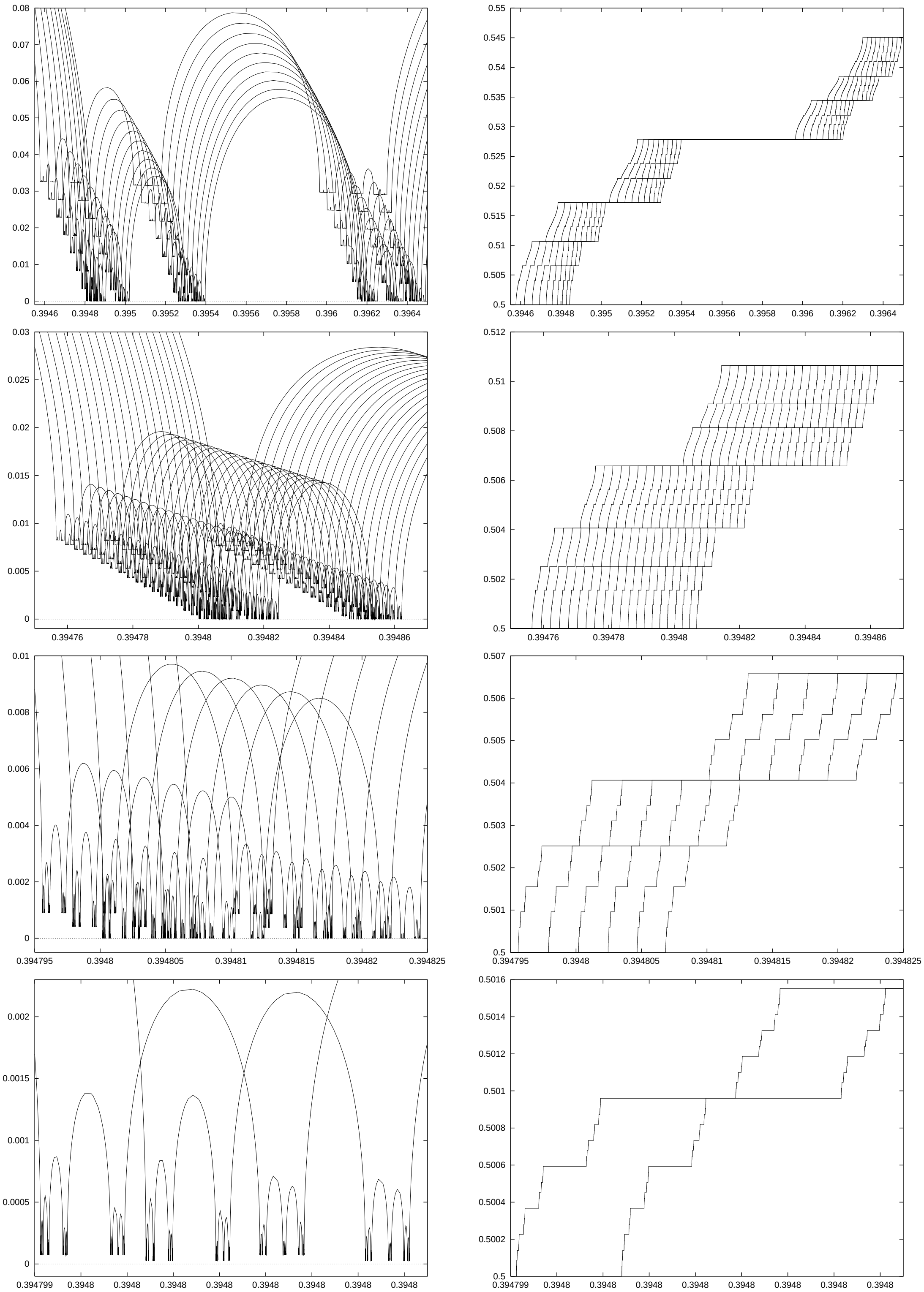

Figure 16: Details of the behavior of λ and ρ close to the collapse line. Left: $\lambda = \lambda(a^2)$, right: $\rho = \rho(a^2)$. The b–values are: 0.526 to 0.535 with step 10^{-3} for the first row; 0.528 to 0.53 with step 10^{-4} for the second one; 0.528 to 0.5285 with step 10^{-4} for the third one; 0.52832 and 0.52833 for the last one. In the lowest row the horizontal window ranges from 0.3947995 to 0.39480035.

resonances used for the figure. It is clear that the bumps have a maximum on the critical value. The magnification shows that the higher the order of the resonance, the sharper the maximum on the critical value of b. This is, again, another expression of the 'collapse of resonances'.

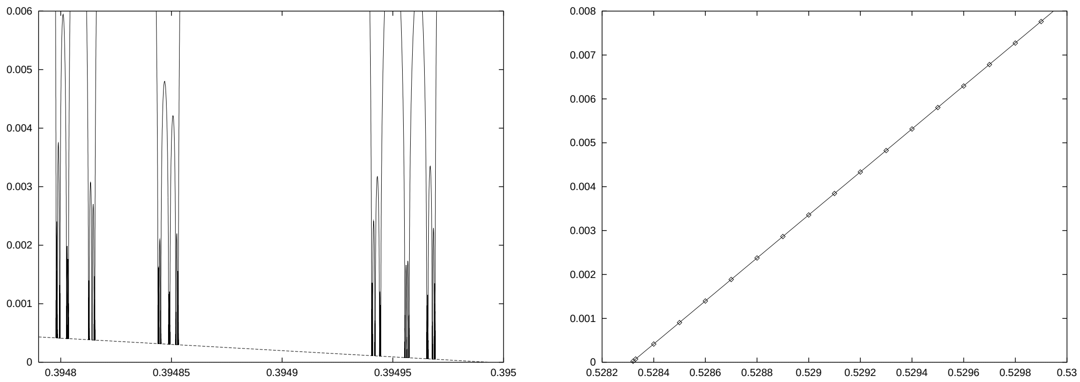

Figure 17: Parameter values for which the right endpoint $a_{1/2,r}$ of the resonance tongue with frequency $\frac{1}{2}$ is on the collapse line. Left: λ as a function of a^2 for $b = 0.5284$ and a fit of the values of $\lambda > 0$ by a line outside the resonance tongues. Right: A measure of the distance of $a^2_{1/2,r}$ to the collapse line as a function of b, and an extrapolation.

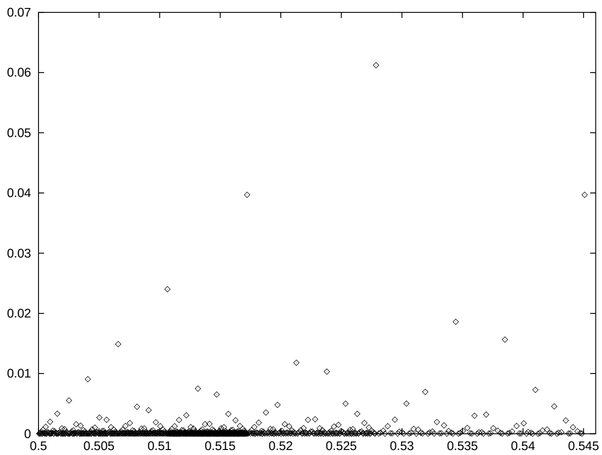

Figure 18: Heights of the bumps in λ as a function of the related frequency for $b = 0.5284$. See the text for additional explanation.

5.4 Breakdown of tori

Similar to what has been done in the previous subsection for the resonance with $\rho = \frac{1}{2}$, we study the behavior of a nonresonant torus when crossing the collapse line, observing its breakdown. We set $\rho = \rho^* = 1/\sqrt{3} \sim 0.577350269$. First we obtained $a_{\rho^*}(b)$, where $\rho(a_{\rho^*}(b), b) = \rho^*$. Also $\lambda(a_{\rho^*}(b), b)$ was computed. Figure 20 shows plots of both functions. It is clearly seen that there is a value, $b_{\text{crit}}(\rho^*)$, up

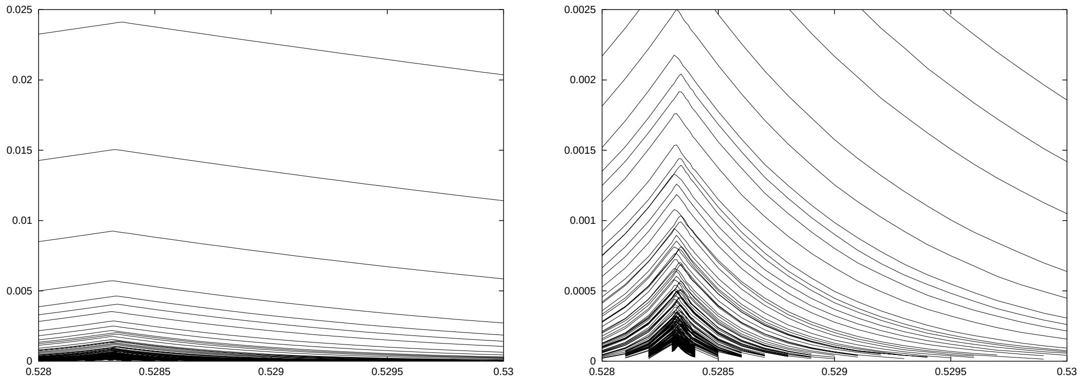

Figure 19: Heights of the bumps in λ as a function of b. The right figure shows a magnification, in the vertical direction, of the left one. See the text for additional explanation.

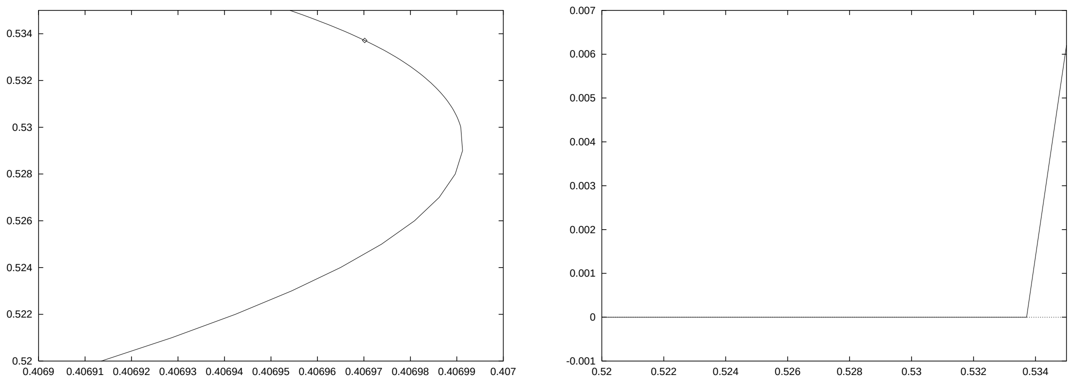

Figure 20: Left: The curve with $\rho = 1/\sqrt{3}$ on the (a^2, b)–plane. The marked point is on the collapse line. Right: Value of $\lambda(b)$ along this curve. It starts to be positive on the collapse line.

to which the corresponding value of λ along the curve $(a_{\rho^*}(b), b)$ is zero and, from that point on, it increases locally almost linearly. The corresponding point of the curve associated to ρ^* is, by definition, on the collapse line. For the given value of ρ^* the approximate value $b_{\text{crit}}(\rho^*) = 0.533713$ has been obtained (in fact it is slightly larger) and then the related value of a (for short $a_{\text{crit}}(\rho^*)$) is ~ 0.40697017905282.

Figure 21 shows a plot similar to figure 18 for the present value of b. Again the disposition of the heights of the bumps in λ along a lattice of lines with scaling properties appears for this critical non-resonant case. In this figure we have skipped two relatively big bumps corresponding to the, comparatively, 'low order' resonances: $(95, -58)$ and $(-49, 31)$. Figure 22 shows a plot of the height of the bumps as a function of the inverse of the order of the related resonance ($|k| = |k_1| + |k_2|$). In this figure a computation with $\delta a^2_{\min} = 10^{-11}$ is able to detect all the harmonics of order less than 20,000 in the selected a–range and most of the harmonics of order up to 2×10^5. The figure reveals a clear linear behavior. A magnification shows that most of the data are concentrated on two nearby lines, the upper one corresponding

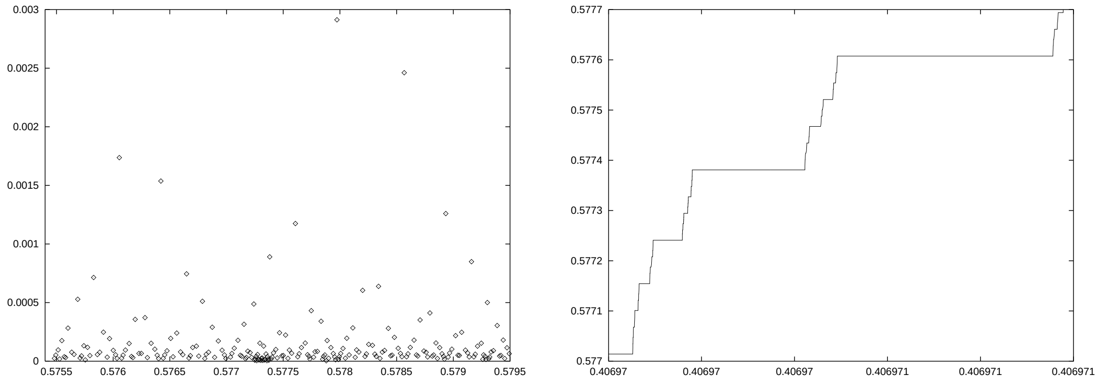

Figure 21: Heights of the bumps in λ as a function of the related frequency for $b = 0.533713$. To the right part, $\rho(a^2)$ on a window of width 10^{-6} in a^2 close to the center of the ν–range of the left figure.

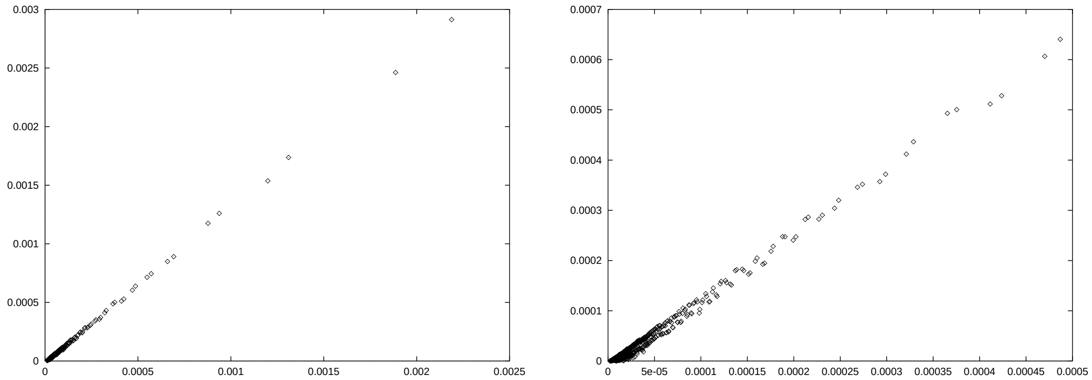

Figure 22: Heights of the bumps found for $b = b_{\text{crit}}(\rho^*)$ for values of a around $a_{\text{crit}}(\rho^*)$, versus $1/|k|$. To the right a magnification.

to $a > a_{\text{crit}}(\rho^*)$ and the lower one to $a < a_{\text{crit}}(\rho^*)$. This behavior can be combined with the fact that the heights of the bumps are roughly proportional to the square roots of the widths of the corresponding instability windows in the a parameter and that a normal form approach gives that the widths are proportional to the amplitude of the harmonics (see the discussion after theorem 2). This illustrates the evidence mentioned at the end of section 4 concerning the behavior of the amplitudes of the harmonics when we approach the collapse line: The amplitude of the harmonic k tends to behave like $1/|k|^2$ for the harmonics giving frequencies which tend to ρ. This would be in favour of a decrease of the regularity of the invariant torus until it is just $\mathcal{C}^1$ (see later).

However figure 22 shows a cloud of data close to the origin. To resolve them we can plot log(height) versus $|k|$. The result can be seen in figure 23. The heights below $\exp(-11)$ do no longer behave like $1/|k|$, but rather they decrease in an exponential way. This shows that, in fact, the value $b = 0.533713$ still has an invariant torus and that, at the end, the coefficients decrease as it corresponds to an analytic torus. Writting height$\sim \exp(-\kappa|k|)$ one can estimate κ to be close to $1/75000$ for this

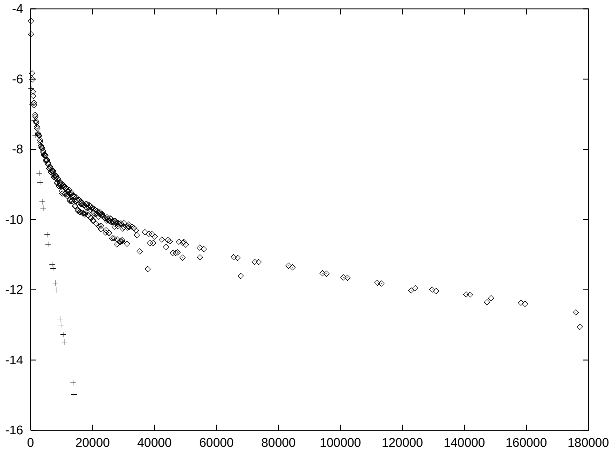

Figure 23: Same as figure 22 but using $|k|$ as horizontal coordinate and the logarithm of the height of the bump as vertical variable. The crosses are the corresponding results for $b = 0.5335$.

value of b. It is interesting to compare with values of b slightly smaller. Even using $b = 0.533$ one has a fast decrease of the heights. Hence we have taken a value of $b = 0.5335$, very close to the previous one, to have a significant number of detectable bumps inside a small range of a around $a_{\rho^*}(b)$. The exponential decrease is clearly seen if we allow to include heights of the order of $\exp(-15)$. The related value of κ can be estimated as $1/200$. Using larger a–domains, to allow for larger bumps, the initial behavior (for small $|k|$) of the height is like $|k|^{-\psi}$ (and, hence, like $|k|^{-2\psi}$ for the size of the harmonics) with $\psi > 1$. Therefore, these numerical results seem to show that the invariant tori, when they exist, are analytic, but going towards a continuous object when the parameters tend to the collapse line.

To see the behavior in the phase space, in figure 24 we show two plots of tori with $\rho = 1/\sqrt{3}$ and b equal to 0.5 and 0.53, respectively. Note that these values are relatively 'far' of the critical one. We also note that the 'size' of the tori is roughly proportional to $1/(b_{\text{crit}}(\rho^*) - b)$. For instance, for $b = 0.533$, a figure similar to the plots in figure 24 requires a minimal window with half widths 1.2×10^3 and 9.7×10^3. No nonlinear terms exist, able to stop this explosion in size! Compare also the torus for $b = 0.53$ with figure 11 3), which shows a typical behavior for the nonresonant case after crossing the collapse line.

6 Conclusions and outlook

Hill's equation with quasi–periodic forcing in some respect is quite similar to the case of periodic forcing. This is particularly true regarding the behaviour of resonance tongues for small forcing. Also the explanation in terms of normal forms (averaging) is similar to the periodic case.

The phenomenon of instability pockets and its explanation was quite new for the periodic case [5, 6] and again, this part of the theory translates to the quasi–periodic case.

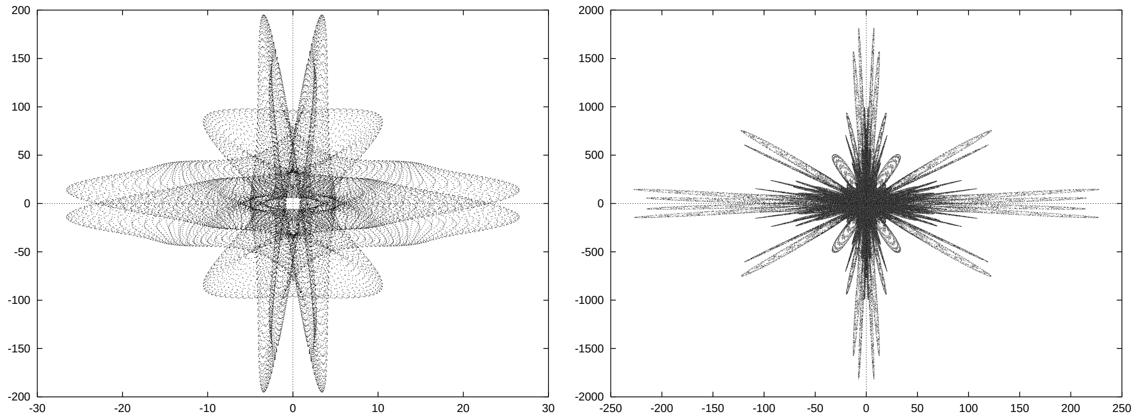

Figure 24: Tori produced as in figure 11. Left: The torus for $b = 0.5$. Right: The torus for $b = 0.53$.

However, in our quasi–periodic case, the behaviour in the complement of the resonance tongues as well as the global behaviour of these tongues is quite different from the periodic case. There is a strong relation with reducibility. To be more precise we have the following, also see the discussion of §1. First, for both $\lambda > 0$ and $\rho \neq \frac{1}{2}(k_1 + k_2\gamma)$, $\forall (k_1, k_2) \in \mathbb{Z}^2$, there can be no reducibility. Second, inside the tongues one has the 'easy' hyperbolic reducibility. Third, for $\lambda = 0$ one can have the 'hard' elliptic reducibility. This has been established only for large values of a, [22, 10]. However, it seems that these results can be carried over to the case of finite a and small b. Indeed, the numerical evidence of the present paper for finite values of (a, b), together with KAM–arguments regarding averaging, see e.g., [1, 17, 22, 10], seem to be in favor of the following facts:

1. For small b, in the (a, b)–plane a Cantor bundle of b–parametrized curves exists, on which elliptic reducibility holds. In the gaps the tongues are sitting, for the rest this bundle has full measure. We refer to this part of the parameter plane as the *KAM–domain*.

   The Cantor bundle is characterized by estimating $|\rho(a, b) - \frac{1}{2} < k, \omega > |$ from below in a diophantine way, as usual. Apart from the above references we like to mention forthcoming work [23].

2. A priori also non–reducibility may occur, in particular when, outside the resonance tongues, $\rho - \frac{1}{2} < k, \omega >$ is a Liouville–like number. This would only occur inside a residual subset of the (a, b)–plane, of measure zero. Again, such considerations hold for small b. It will be interesting to test the present examples of p for this phenomenon, but also to widen the class, e.g., by introducing extra parameters. Compare with [15, 12].

   Note that the results of this endeavour may cast some doubt on Conjecture 3.

3. The KAM–domain reaches until the 'collapse line', where a breakdown of the nontrivial KAM–tori occurs. From this line on, the dynamics is only reducible

inside the resonance tongues.

4. At the collapse line the resonance tongues seem to increase so much in width, that no space is left over for nontrivial tori.

Several generalizations also seem worth investigating. Let $r = \omega_2/\omega_1$ be the ratio of frequencies.

- What happens if the frequency–ratio r tends to some rational value, but ranging over the set of diophantine numbers? One expects to recover the classical Floquet–theory for periodic solutions. One may guess that the collapse line then should disappear to ∞ in the b direction.

- How does the over–all picture change if the frequency–ratio r is non–diophantine, but e.g., a Liouville number?

- How does the existence of instability pockets interfere with the collapse line?

- What is the generic situation when $p(t)$ is quasi–periodic with 3 or more basic frequencies?

- Hill's equation with quasi–periodic forcing probably is the simplest example of a linear equation with quasi–periodic coefficients. What could be expected for general equations in $\mathbb{R}^n$?

A Appendix

In this Appendix we describe the methods used for the numerical computations. The main goal is to achieve good accuracy with small computing time. Indeed, accuracy is required to produce realiable numerical results. Taking as unit of computing time the evaluation of one iterate of (5), and the estimate of λ and ρ when being beyond some initial transient, the total number of units used in our explorations is close to 10^{13}. Only a very small selection has been displayed here. This large number asks for fast computations. An important part of the task has been carried out on a Beowulf cluster consisting of 24 Pentium 266 processors and 2 Pentium 200 processors. Each processor is able to do near 2×10^5 iterates per second.

A.1 Computation of $M(\theta)$

We have to integrate an equation of the form $\ddot{x} = q(t)x$. In the present case $q(t) = -(a^2 + b(\cos(t) + \cos(\gamma t + \theta)),\ \gamma = \frac{1}{2}(1+\sqrt{5})$, and, for most of the computations, a and b have been confined to $[0, 1]$.

Let us introduce $x^{(k)} = \frac{1}{k!}\frac{d^k x}{dt^k}$. In a similar way we introduce $q^{(k)}$. Then, the Leibnitz rule gives the relation

$$x^{(k+2)} = \frac{1}{(k+1)(k+2)}\Sigma_{j=0}^{k} x^{(k-j)} q^{(k)},$$

allowing to compute recurrently all $x^{(k)}$ up to any order N, with a computational cost $O(N^2)$, starting from $x^{(0)}$ and $y^{(0)} = x^{(1)}$. The 'trigonometric' cost is only two evaluations of cos and sin per step, the powers of γ and the inverse of the factorials being computed just once.

The series for $x(t+h)$, as a function of h, starting from $x(t), y(t)$ is majorated by the one of $\ddot{z}(h) = r(h)z(h)$, where $r(h) = a^2 + |b|\,(\exp(h) + \exp(\gamma h))$, starting from $z(0) = |x(t)|, \dot{z}(0) = |y(t)|$. This shows that the series is entire. Furthermore, if we restrict a and b as declared and take $h < 1$, then $r(h) < 9$. Hence $z(h) < A\exp(3h)$, where A depends on $z(0)$ and $\dot{z}(0)$. This shows that selecting, say, $N = 30$, the last term is less than 10^{-18} times the larger of the first two.

In fact we integrate the equation starting at $(1,0)$ and $(0,1)$. We have selected a constant time step (typically $2\pi/8$ or $2\pi/10$ give optimal computing time) and select N such that the maximum of the 2 last terms appearing in the expansions of the 4 places of the fundamental matrix is less than 10^{-18} times the maximum of the absolute values of the elements of the matrix.

This computation is done for a large number, K, of θ–values, equally spaced in $[0, 2\pi]$. For refined computations, where we are interested in a large number of iterates, $K = 5000$ is a suitable choice. The large initialization time (typically 3 seconds) allows to reduce the computing time in the iterations.

A.2 The interpolation process

We know $M(\theta_k)$, $\theta_k = 2\pi k/K$, $k = 0, \ldots, K-1$, and we have to compute $M(\theta)$. This is done by interpolation. By scaling and shifting the origin we can always assume that we have to evaluate a function, $f(s)$, at some point $s \in [0,1)$ from the values $f_j = f(j)$, $j = 1-j_0, \ldots, j_0$. The interpolation formula is of the form $\Sigma_{j=1-j_0}^{j_0} w_j(s) f_j$, where $w_j(s)$ are the Lagrangian weights. To speed up the process even further, the weights, $w_{j,i}$, for $s = i/10000$, $i = 0, \ldots, 10000$ have been precomputed. Then the corresponding weights $w_j(s)$ are obtained from the precomputed weights by linear interpolation. It has been checked that this produces no significant differences in the computation of $M(\theta)$. The interpolation has to be applied to each of the elements of the matrix. A suitable value for j_0 is 3. So, just 6 nodes are used for the interpolation. Numerical estimates of the 6–th derivative of the elements of $M(\theta)$ in preliminary runs show that the error estimates in the interpolation formula are of the order of the ϵ of the computer.

A.3 Estimates of λ and ρ

The formulas (6) and (7) define λ and ρ whenever the limits exist. However, to have good enough estimates it is possible that the number n of iterates has to be taken very large, due to 'irregular' behavior of these iterates. Figure 25 shows a related example, displaying the quotient appearing in (6) after a large transient, to be explained further below. A typical value for the number of iterates in the transient, in the region close to the collapse line, is 10^6. The maximum of iterates

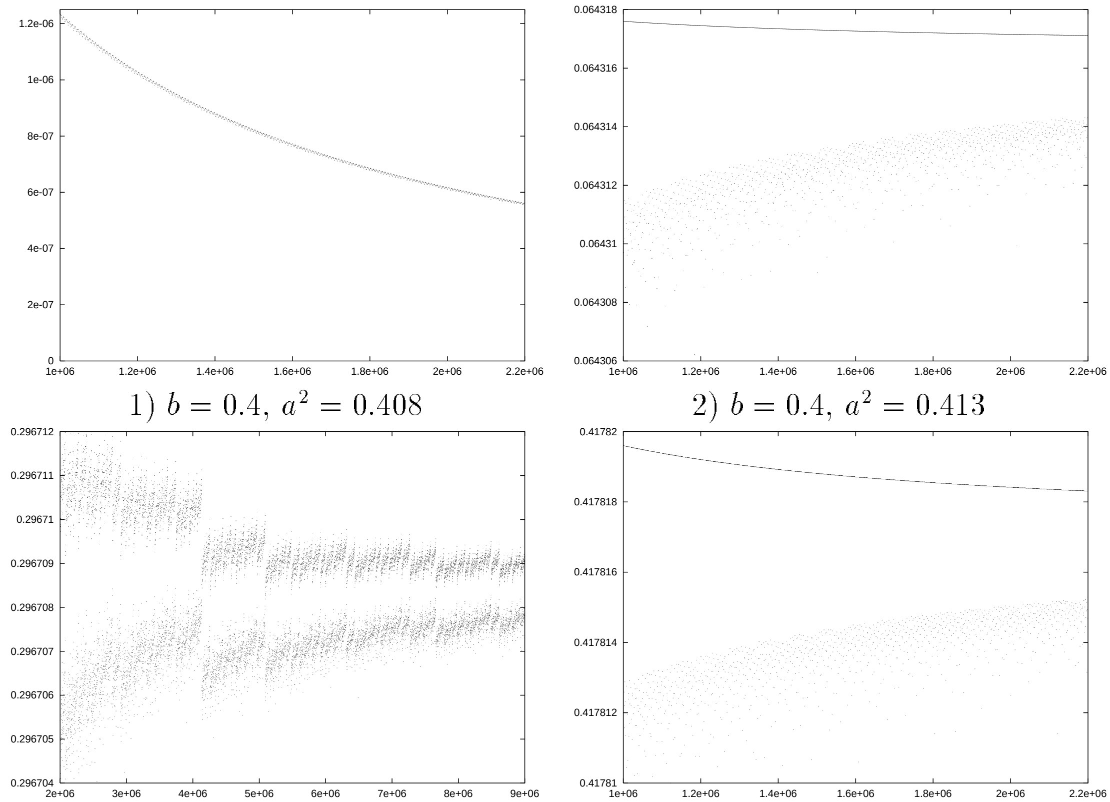

1) $b = 0.4,\ a^2 = 0.408$ 2) $b = 0.4,\ a^2 = 0.413$

3) $b = 0.6,\ a^2 = 0.408$ 4) $b = 0.6,\ a^2 = 0.413$

Figure 25: Estimates of λ as a function of the number of iterates for the (a, b)–values shown. In all cases the maxima and minima in blocks of 10^3 iterates are displayed. In 1) we only show the maxima, the minima being below 2.1×10^{-16}. Notice that in 3), for parameters above the collapse line and outside resonance, the behavior is even more irregular, despite the transient of 2×10^6 iterates and the additional 7×10^6 iterates computed. However, it seems that, even in this case, lim inf and lim sup, of the estimates of λ, coincide.

has been set to 10^7. Guided by the results summarized in section 5 and by the behavior observed in many plots of the estimates, the following heuristic approach has proved itself to be suitable to estimate λ. It was also used for ρ, despite the fact that the quotients in (7) show more regularity.

After a transient, which in some cases has to go up to 2×10^6 iterates, the quotients of (6) are computed after each iterate, but only the largest quotient in blocks of, say, 1,000 consecutive iterates are recorded. The number of the iteration where the maximum takes place is also recorded. Then, after computing a number of blocks (say, 100 blocks and then, in successive estimates, 200, 300, etc, blocks are used) a fit of the values at the maxima by an expression of the form $\lambda_{n_i} = \alpha + \beta/n_i$ is done. Here n_i is the number of the iteration where the maxima occur and λ_{n_i} the related quotient. The value of α gives an improved estimate of the Lyapunov exponent.

Anyway, comparing successive improved estimates shows that still the convergence (is any!) is too slow. Then we do again an iterative process. After the fit has been done, we discard all the points below the fitting curve, produce a new fit with the points which remain, discard again, etc, until the number of points used in the last fit is not less than some number. In practice this number has been taken as 50. The value of α of this last fit is used as estimate of λ. It was observed that these estimates are much more coherent when the number of blocks increases. When 3 successive estimates obtained in this way differ by less than some tolerance (10^{-8} was taken for the best refinements) the last one is used as final estimate of λ.

Looking at the results for (a, b) values such that it seems clear that λ must be zero, the results obtained in this way are always less than 10^{-8} and, in most of the cases, even below 10^{-10}. Also in the resonant zones the behavior is smooth within 10^{-8} (e.g., looking at the finite differences for equally spaced values of a^2.) In domains outside the resonant tongues, above the collapse line, the behavior is also smooth within this tolerance. Only near the crossing of the collapse line it seems that a few estimates can have errors up to, at most, 10^{-6}.

A.4 The scanning process

Up to now we described how to obtain λ and ρ for given values of (a, b). Fixing b we produced estimates for a ranging on a given interval. For this 'scanning process' the following rules have been used. We chose some tolerances δ_λ and δ_ρ, such that if the selected values of a^2, at which the computations are done, are labelled as a_j^2, $a_j^2 < a_{j+1}^2$, then $|\lambda(a_{j+1}^2) - \lambda(a_j^2)| < \delta_\lambda$ and $|\rho(a_{j+1}^2) - \rho(a_j^2)| < \delta_\rho$, unless this forces to take $a_{j+1}^2 - a_j^2 < \delta a_{\min}^2$. Typical choices for details are $\delta_\lambda = 10^{-4}$, $\delta_\rho = 10^{-5}$, $\delta a_{\min}^2 = 10^{-11}$. These values were selected in order not to miss most of the details of the plots of λ and ρ and, at the same time, to progress efficiently in the scanning.

A.5 The Fourier analysis

As mentioned in section 5, to carry out a Fourier analysis of the results in the phase space, we first have cancelled the eventual exponential increase of the iterates. This is done by computing, after the initial transient, the matrices $\hat{P}_n = \exp(-n\lambda)P_n$, where the P_n are the fundamental matrices after a time of $2\pi n$. (See after formula (5)).

We consider just one of the vectors of the $\hat{P}_n$ matrices. To be precise, we used the first vector. If the equation is reducible to constant coefficients (Floquet form), the Fourier analysis of that vector should contain the harmonics involved in the change of variable (whose frequencies must be integer linear combinations of the fundamental ones) and the ones coming from the frequency associated to the reduced matrix.

Typically we used the first 2^{18} iterates after the transient to carry out the Fourier analysis. Then a FFT routine reveals the dominant harmonics. We refer to section 5 for some plots. To locate the main frequencies several refined methods are available (e.g. [20], [21], [14]). However even a simpler method can be used because the basic frequencies are known and the frequency associated to the eventually reduced equation is approximated by ρ. The identification of frequencies of the main harmonics, in the cases which look as reducible, is done with errors below 10^{-7}.

Acknowledgements

The authors thank Hans Jauslin for suggesting this problem to both of them and for stimulating exchange of ideas. They also thank Russell Johnson, Àngel Jorba and Yingfei Yi for helpful discussion. The research of the second author has been supported by DGICYT grant PB 94–0215 (Spain). Partial support of the EC grant ERBCHRXCT940460, and the catalan grant CIRIT 1996S0GR-00105 also is acknowledged.

References

[1] Braaksma, B.L.J. and Broer, H.W.: On a quasi–periodic Hopf bifurcation, *Ann. Institut Henri Poincaré, Analyse non Linéaire* **4**(2), (1987), 115–168.

[2] Broer, H.W., Hoveijn, I. and van Noort, M.: A reversible bifurcation analysis of the inverted pendulum, *Physica D*, **112**, (1997), 50–63.

[3] Broer, H.W., Huitema, G.B., Takens, F. and Braaksma, B.L.J.: Unfoldings and bifurcations of quasi-periodic tori. *Mem AMS* **83**(421), 1990.

[4] Broer, H.W., Huitema, G.B. and Sevryuk, M.B.: *Quasi–periodic motions in families of dynamical systems, order amidst chaos*. LNM **1645** Springer–Verlag, 1996.

[5] Broer, H.W. and Levi, M.: Geometrical aspects of stability theory for Hill's equations. *Arch. Rat. Mech. An.* **131** (1995), 225-240.

[6] Broer, H.W. and Simó, C.: Resonance tongues in Hill's equations: a geometric approach, preprint, 1997.

[7] Broer, H.W. and Vegter, G.: Bifurcational aspects of parametric resonance. *Dynamics Reported, New Series* **1** (1992), 1–51.

[8] Broer, H.W., Takens, F. and Wagener, F.O.O.: Unfolding the skew Hopf bifurcation, preprint, 1998.

[9] Broer, H.W. and Wagener, F.O.O.: Quasi–periodic stability of subfamilies of an unfolded skew Hopf bifurcation, preprint, 1998.

[10] Eliasson, L. H.: Floquet solutions for the 1–dimensional quasi-periodic Schrödinger equation. *Commun. Math. Phys.* **146** (1991), 447–482.

[11] Eliasson, L. H.: Ergodic skew systems on $\mathbb{T}^d \times SO(3, \mathbb{R})$, preprint, 1996.

[12] Fabbri, R., Johnson, R. and Pavani, R: On the spectrum of the quasi–periodic Schrödinger operator. In preparation.

[13] Giorgilli, A. and Galgani, L.: Formal integrals for an autonomous Hamiltonian system near an equilibrium point. *Celest. Mech.* **17** (1978), 267–280.

[14] Gómez, G., Llibre, J., Martínez, R. and Simó, C.: *Study on orbits near the triangular libration point in the perturbed restricted three-body problem.* ESA Technical Report, 1987, 270p.

[15] Johnson, R.: Cantor spectrum for the quasi–periodic Schrödinger operator. *J. Diff. Eqns.* **91** (1991), 88–110.

[16] Jorba, À., Ramírez–Ros, R. and Villanueva, J.: Effective Reducibility of Quasiperiodic Linear Equations Close to Constant Coefficients, *SIAM J. on Math. Anal.* **28** (1996), 178–188.

[17] Jorba, À. and Simó, C.: On the reducibility of linear differential equations with quasiperiodic coefficients. *J. Diff. Eq.* **98** (1992), 111–124.

[18] Jorba, À. and Simó, C.: On quasiperiodic perturbations of elliptic equilibrium points, *SIAM J. of Math. Anal.* **27** (1996), 1704–1737.

[19] Krikorian, R.: Réductibilité presque partout des flots fibrés quasi–périodiques à valeurs dans des groupes compacts, preprint, 1996.

[20] Laskar,J.: The chaotic motion of the solar system. A numerical estimate of the size of the chaotic zones, *Icarus* **88** (1990), 266–291.

[21] Laskar,J., Froeschlé, C., Celletti, A.: The measure of chaos by the numerical analysis of the fundamental frequencies. Application to the standard mapping, *Physica D* **56** (1992), 253–269.

[22] Moser, J. and Pöschel, J.: An extension of a result by Dinaburg and Sinai on quasi–periodic potentials, *Comment. Math. Helvetici* **59** (1984), 39–85.

[23] Wagener, F.O.O.: On a.e. reducibility of quasi–periodically perturbed two–dimensional Floquet systems. In preparation.